Available online at www.sciencedirect.com
ScienceDirect
Geochimica et Cosmochimica Acta 75 (2011) 5797–5818
Geochimica et Cosmochimica Acta
www.elsevier.com/locate/gca

Magnesium stable isotope fractionation in marine biogenic calcite and aragonite

F. Wombacher [a,b,c,*], A. Eisenhauer [a], F. Böhm [a], N. Gussone [a,d], M. Regenberg [a,e], W.-Chr. Dullo [a], A. Rüggeberg [a,f]

[a] IFM-GEOMAR Leibniz-Institut für Meereswissenschaften, Wischhofstr. 1-3, D-24148 Kiel, Germany
[b] Institut für Geologische Wissenschaften, FR Geochemie, Freie Universität Berlin, Malteserstr. 74-100, D-12249 Berlin, Germany
[c] Institut für Geologie und Mineralogie, Universität zu Köln, Zülpicher Str. 49b, D-50674 Köln, Germany
[d] Institut für Mineralogie, Universität Münster, Corrensstr. 24, D-48149 Münster, Germany
[e] Institut für Geowissenschaften, Christian-Albrechts-Universität, Ludewig-Meyn-Str. 10-14, D-24118 Kiel, Germany
[f] Renard Centre of Marine Geology, Ghent University, Krijgslaan 281, S8, B-9000 Gent, Belgium

Received 7 September 2010; accepted in revised form 14 July 2011; available online 23 July 2011

Abstract

This survey of magnesium stable isotope compositions in marine biogenic aragonite and calcite includes samples from corals, sclerosponges, benthic porcelaneous and planktonic perforate foraminifera, coccolith oozes, red algae, and an echinoid and brachiopod test. The analyses were carried out using MC-ICP-MS with an external repeatability of ±0.22‰ (2SD for δ^{26}Mg; $n = 37$), obtained from a coral reference sample (JCp-1).

Magnesium isotope fractionation in calcitic corals and sclerosponges agrees with published data for calcitic speleothems with an average $\Delta^{26}Mg_{calcite-seawater} = -2.6 \pm 0.3‰$ that appears to be weakly related to temperature. With one exception (*Vaceletia* spp.), aragonitic corals and sclerosponges also display uniform Mg isotope fractionations relative to seawater with $\Delta^{26}Mg_{biogenic\ aragonite-seawater} = -0.9 \pm 0.2$.

Magnesium isotopes in high-Mg calcites from red algae, echinoids and perhaps some porcelaneous foraminifera as well as in all low-Mg calcites (perforate foraminifera, coccoliths and brachiopods) display significant biological influences. For planktonic foraminifera, the Mg isotope data is consistent with the fixation of Mg by organic material under equilibrium conditions, but appears to be inconsistent with Mg removal from vacuoles. Our preferred model, however, suggests that planktonic foraminifera synthesize biomolecules that increase the energetic barrier for Mg incorporation. In this model, the need to remove large quantities of Mg from vacuole solutions is avoided. For the high-Mg calcites from echinoids, the precipitation of amorphous calcium carbonate may be responsible for their weaker Mg isotope fractionation.

Disregarding superimposed biological effects, it appears that cation light isotope enrichments in $CaCO_3$ principally result from a chemical kinetic isotope effect, related to the incorporation of cations at kink sites. In this model, the systematics of cation isotope fractionations in $CaCO_3$ relate to the activation energy required for cation incorporation, which probably reflects the dehydration of the cation and the crystal surface and bond formation at the incorporation site. This kinetic incorporation model predicts (i) no intrinsic dependence on growth rate, unless significant back reaction upon slow growth reduces the isotope fractionation towards that characteristic for equilibrium isotope partitioning (this may be observed for Ca isotopes in calcites), (ii) a small decrease of isotope fractionation with increasing temperature that may be amplified if higher temperatures promote back reaction and (iii) a sensitivity to changes in the activation barrier caused by additives such as anions or biomolecules or by the initial formation of amorphous $CaCO_3$.

* Corresponding author at: Institut für Geologie und Mineralogie, Universität zu Köln, Zülpicher Str. 49b, D-50674 Köln, Germany. Tel.: +49 221 470 3197.
E-mail address: fwombach@uni-koeln.de (F. Wombacher).

0016-7037/$ - see front matter © 2011 Elsevier Ltd. All rights reserved.
doi:10.1016/j.gca.2011.07.017

1. INTRODUCTION

Magnesium is present in biogenic marine $CaCO_3$, with $MgCO_3$ abundances of 4 to ~30 mol % in high-Mg calcites (HMC), <4 mol % in low-Mg calcites (LMC) and typically <0.6 mol % in aragonites (e.g. Tucker, 2001; Flügel, 2004). The presence of Mg exerts a strong control on the inorganic and biogenic precipitation of $CaCO_3$. Experiments on $CaCO_3$ precipitation showed that high Mg contents in solution impede calcite formation (Berner, 1975; Mucci and Morse, 1984; Davis et al., 2000; Astilleros et al., 2010). As a consequence, metastable aragonite commonly forms in Mg-rich solutions (Mucci and Morse, 1984) and together with HMC at times of high Mg/Ca seawater compositions (aragonite seas, e.g. Hardie, 1996; Stanley, 2006). The extent of Mg substitution in $CaCO_3$ is temperature dependent (Mucci, 1987) and this property is exploited in numerous reconstructions of past sea water temperatures, often based on foraminiferal calcite (e.g. Nürnberg et al., 1996; Rosenthal et al., 1997).

Stable carbon and oxygen isotope distributions have been studied extensively in biogenic $CaCO_3$ and applied in the reconstruction of paleoenvironmental conditions as well as for investigations of biomineralization processes. In contrast, the stable isotope geochemistry of alkaline and earth alkaline cations in $CaCO_3$ mainly emerged after 2000. A few studies focused on Li (Marriott et al., 2004a,b) and Sr isotopes (Fietzke and Eisenhauer, 2006; Rüggeberg et al., 2008), while the largest number of studies so far focused on Ca isotope compositions in $CaCO_3$ from inorganic precipitation experiments (Gussone et al., 2003; Lemarchand et al., 2004; Tang et al., 2008) and biogenic $CaCO_3$ (e.g. Skulan et al., 1997; Nägler et al., 2000; Sime et al., 2005; Böhm et al., 2006; Gussone et al., 2006; Langer et al., 2007; Rollion-Bard et al., 2007; Griffith et al., 2008a; Kasemann et al., 2008; Kisakürek et al., 2011). Following the development of suitable analytical methods by MC-ICP-MS (Galy et al., 2001; Chang et al., 2003), a range of about 4‰ was observed for $^{26}Mg/^{24}Mg$ isotope compositions in $CaCO_3$, with the light isotopes always enriched in the mineral phase (Galy et al., 2002; Chang et al., 2004; Buhl et al., 2007; Pogge von Strandmann, 2008; Hippler et al., 2009; Immenhauser et al., 2010; Higgins and Schrag, 2010; Ra et al., 2010; Rose-Koga and Albarède, 2010; Müller et al., 2011).

Galy et al. (2002), Buhl et al. (2007) and Immenhauser et al. (2010) investigated the Mg isotope compositions in speleothems. Relative to the associated drip waters Galy et al. (2002) observed a light isotope enrichment of −2.7‰ for $\Delta^{26}Mg$ in calcite. A speleothem containing dolomite and dolostones displayed heavier Mg isotope compositions compared to limestones, suggesting a strong mineralogical control of Mg isotope fractionation in carbonate rocks and minerals. Chang et al. (2004), Pogge von Strandmann (2008) and Hippler et al. (2009) report data for recent biogenic calcites. While red algae samples and one calcitic coral displayed only slightly weaker Mg isotope fractionations compared to speleothem calcite, the light Mg isotope enrichment in echinoids and brachiopods were observed to be significantly smaller due to biological effects. Bivalve samples (*Mytilus edulis*), however, displayed stronger and more variable Mg isotope fractionations. Calcitic foraminifera are even more enriched in the light Mg isotopes, with typical $\Delta^{26}Mg$ in the range of −4‰ to −5‰ due to additional biological effects (Chang et al., 2004; Dessert et al., 2005; Pogge von Strandmann, 2008). Speleothem calcite, echinoids, red algae, foraminifera and bivalves display no clearly resolvable relationship between Mg isotope compositions and temperature (Galy et al., 2002; Pogge von Strandmann, 2008; Hippler et al., 2009), but Mg isotopes in coccoliths from *Emiliania huxleyi* correlate with temperature and growth rate (Ra et al., 2010). The few published Mg stable isotope data available for coral and scaphopod aragonite display much smaller light Mg isotope enrichments of about −0.9‰ to −1.3‰ relative to seawater, which suggests a mineralogical effect (Chang et al., 2004; Dessert et al., 2005; Hippler et al., 2009).

The prominent role of Mg for $CaCO_3$ precipitation, the widespread use of Mg/Ca in paleoceanography, the potential of cation stable isotopes as proxies and the sometimes apparently inconsistent results from these isotope systems call for a closer look at Mg stable isotope fractionations in $CaCO_3$. Here we report precise Mg isotope data for biogenic aragonite (corals and sponges) as well as high and low-Mg calcite (corals, sponges, benthic porcelaneous and planktonic perforate foraminifera, coccolith ooze, an echinoid, a red algae and one brachiopod). Part of the data has been reported in abstract form (Wombacher et al., 2006). The data combined with some of the literature data cited above is used to further evaluate (i) the mechanisms for cation isotope fractionation during inorganic $CaCO_3$ precipitation, (ii) biological influences on Mg isotope fractionation in $CaCO_3$, and (iii) the potential of Mg isotopes as paleoceanographic proxies.

2. SAMPLES, PREPARATION AND ANALYSIS

2.1. Samples and preparation

2.1.1. Aragonite

The aragonite sample set comprises warm and cold-water corals and sclerosponges. The warm water corals include *Porites* sp. and *Porites lutea*. The *Porites* sp. sample is a powdered reference material (JCp-1) obtained from the Japanese Geological Survey (Okai et al., 2003). *P. lutea* samples are obtained from drill cores from a large living specimen at the Gulf of Aqaba/Red Sea (sample 19/1 of Heiss et al., 1999). Slabs from the drill core were cleaned in 10% H_2O_2 for 48 h to remove organic matter (Heiss et al., 1999). Sample 1a was microdrilled from the high-density band that correspond to the colder season (presumably grown in 1991), while sample 1b was collected from a less dense band corresponding to the preceding warmer season. This is reflected in the sea water temperatures of 23.8 and 20.8 °C, respectively (Table 1) calculated from O isotope compositions obtained on sample aliquots and the equation given in Heiss et al. (1999).

The azooxanthellate cold-water corals, *Lophelia pertusa* and *Desmophyllum dianthus* (aka *D. cristagalli*) were obtained from the NE Atlantic, west of Ireland during Meteor

Table 1
Magnesium stable isotope compositions of biogenic $CaCO_3$ relative to DSM3.

Sample (id[a])	$\delta^{26}Mg$	$\delta^{25}Mg$	$\delta^{18}O$[b]	T (°C)
Aragonite				
Corals				
Porites sp. (JCp-1)[c]	−2.01	−1.05		25
Porites lutea #1a	−1.76	−0.93	−2.94 ± 0.04	23.8
Porites lutea #1a	−1.82	−0.95		23.8
Porites lutea #1b	−1.83	−0.92	−2.40 ± 0.08	20.6
Lophelia pertusa #1a	−1.52	−0.85		8.8
Lophelia pertusa #1a	−1.68	−0.87		8.8
Lophelia pertusa #1b	−1.58	−0.84		8.8
Lophelia pertusa #2a	−1.73	−0.87		9.0
Lophelia pertusa #2b	−1.74	−0.90		9.0
Desmophylum dianthus	−1.78	−0.96		9.5
Sponges				
Astrosclera willeyana	−1.63	−0.81		26
Astrosclera willeyana	−1.79	−0.94		26
Ceratoporella nicholsoni #1a (Ce95-2)	−1.50	−0.76	−1.04 ± 0.14	28
Ceratoporella nicholsoni #1b (Ce95-2)	−1.53	−0.81	−0.80 ± 0.10	27
Vaceletia sp. #1a (DW398-1)	−2.71	−1.41		16
Vaceletia sp. #1a (DW398-1)	−2.58	−1.37		16
Vaceletia sp. #1a (DW398-1)	−2.55	−1.35		16
Vaceletia sp. #1b (DW398-2)	−3.22	−1.68		16
Vaceletia sp. #1b (DW398-2)	−3.17	−1.68		16
Vaceletia sp. #1b (DW398-2)	−2.98	−1.55		16
Vaceletia sp. #2 (DW 546)	−1.75	−0.91		23
Vaceletia crypta (V4)	−3.10	−1.63		27
Vaceletia crypta (V4)	−3.01	−1.59		27
High Mg calcite (*HMC*)				
Corals				
Keratoisis sp.	−3.38	−1.70	−1.13 ± 0.17	7.5
Keratoisis sp.	−3.52	−1.80		7.5
Sponges				
Acanthochaetetes wellsi#1a (AW92)	−3.30	−1.70		24
Acanthochaetetes wellsi#1b (AW92)	−3.22	−1.65	−0.66 ± 0.06	24
Acanthochaetetes wellsi#1b (AW92)	−3.17	−1.67		24
Acanthochaetetes wellsi #2a (AW Mac)	−3.38	−1.77		27.6
Acanthochaetetes wellsi #2b (AW Mac)	−3.19	−1.65	−1.61 ± 0.11	27.6
Acanthochaetetes wellsi #2b (AW Mac)	−3.22	−1.66		27.6
Coralline red algae				
Lithothamnion glaciale	−3.22	−1.70	−0.59 ± 0.07	7
L. glaciale or other red algae species	−3.14	−1.60	0.18 ± 0.11	7
L. glaciale or other red algae species	−3.19	−1.65		7
Echinoid				
Diadema setosum (ambulacral plate)	−2.48	−1.35		22
Diadema setosum (interamb. plate)	−2.39	−1.28		22
Diadema setosum (interamb. plate)	−2.42	−1.23		22
Diadema setosum (interamb. plate) [d]	−2.47	−1.27		22
Miliolid benthic foraminifera				
Pyrgo sp. (BFII)	−3.17	−1.66		−1
Pyrgo sp. (BFII)	−3.25	−1.75		−1
Pyrgo sp. (BFII)	−3.31	−1.67		−1
Pyrgo sp. (BFII)	−3.32	−1.77		−1
Pyrgo rotalaria	−2.82	−1.44		−1.0
Pyrgo rotalaria	−2.73	−1.44		−1.0
Pyrgo rotalaria	−2.48	−1.29		−1.0
Triloculina sp.	−3.49	−1.78		4.1
3 miliolid species	−3.67	−1.89		4.1

(*continued on next page*)

Table 1 (*continued*)

Sample (id[a])	δ^{26}Mg	δ^{25}Mg	δ^{18}O[b]	*T* (°C)
Low Mg calcite (LMC)				
Planktonic foraminifera				
Neogloboquadrina dutertrei	−4.61	−2.44		23.1
Neogloboquadrina dutertrei	−4.66	−2.40		23.1
Globorotalia menardii	−4.15	−2.20		24.2
Globorotalia menardii	−4.15	−2.14		24.2
Globorotalia menardii	−3.98	−2.10		24.2
Globigerinoides sacculifer	−5.51	−2.85		27.1
Globigerinoides sacculifer	−5.57	−2.84		27.1
Globigerinoides ruber pink	−4.79	−2.45		28.4
Globigerinoides ruber pink	−4.81	−2.50		28.4
Globigerinoides ruber pink	−4.63	−2.45		28.4
Globigerinoides ruber pink	−4.55	−2.38		28.4
Coccolith ooze				
P44	−1.04	−0.55		25
P44[d]	−1.28	−0.66		25
P44[d]	−1.17	−0.64		25
P44[d]	−1.12	−0.62		25
C56	−2.47	−1.32		31
C56	−2.44	−1.25		31
C149[e]	−2.98	−1.54		32.8
C149[e]	−3.05	−1.65		32.8
Brachipod				
Brachiopod	−2.18	−1.11		9.5
Brachiopod	−2.13	−1.13		9.5
Brachiopod[d]	−1.97	−1.01		9.5
Brachiopod[d]	−2.02	−1.04		9.5

[a] Sample identifier in previous publications, see references in text.
[b] Relative to Vienna PDB; average value and uncertainty (1SE) from two analysis.
[c] Coral reference material from Japanese Geol. Soc.; average value taken from Wombacher et al. (2009); external reproducibility of ±0.22 (δ^{26}Mg; 2SD) is estimated from 37 analysis of JCp-1.
[d] Bleached.
[e] Rinsed.

cruise M61. The two living specimens of *L. pertusa* were collected from the Franken Mound, south-west Rockall Bank (#1a and b; M61/3-614 – GeoB 9267, ca. 650 m water depth) and from the Little Galway Mound at the eastern Porcupine Seabight (#2a and b; M61/1-218 BG4, ca. 880 m water depth), respectively. Water temperatures were measured in situ with a CTD probe at the same sites, during the same cruises. Samples #1a and #2a were taken from the outer surface of a branch; sample #1b and #2b were drilled from the center of the branches. A dead specimen of another cold-water coral, *D. dianthus* was obtained from the Kiel Mount, SW Rockall Bank (M61/1-301, at 850–900 m water depth). Two samples have been drilled from this specimen, one from the basal (older) and one from the upper (younger) part of the polyp. The water temperature of 9.5 °C was measured in situ with a CTD probe.

Five specimens of aragonitic sclerosponges were sampled. *Astrosclera willeyana* was obtained from the Gulf of Aqaba, Red Sea (Wörheide, 1998), *Ceratoporella nicholsoni* from Jamaica (Böhm et al., 2000, 2002), the two *Vaceletia* sp. samples are from Lifou/New Caledonia and Wallis et Futuna and *Vaceletia crypta* is from Lizard Island/Great Barrier Reef. For the two drill samples from *C. nicholsoni*, water temperatures of 27 and 28 °C were calculated from O isotopes on sample powder aliquots according to Böhm et al. (2000). Other temperature estimates are from Gussone et al. (2005) and references therein and either calculated from O isotope analyses on different parts of the samples or from the World Ocean Atlas (Conkright et al., 1998). All sponges were alive before collection at 10–30 m water depths, with the possible exception of the *Vaceletia* sp. samples which were dredged from greater depth and may have been dead before sampling.

2.1.2. High-Mg calcite (HMC)

Living *Keratoisis* sp., an azooxanthellate cold-water isidid gorgonian coral (Octocorallia), also referred to as "bamboo coral", has been dredged during RV Sonne cruise SO168 ZEALANDIA from the south-western slope of the Chatham Rise east of New Zealand (station 104; depth between 594 and 770 m) (Noé and Dullo, 2006). A microdrill sample was collected from the calcitic internode. The comparison with a temperature profile taken at the southern Hikurangi Plateau during the same cruise yields a temperature estimate of 7.5 °C with an estimated uncertainty of about ±1 °C (Hoernle et al., 2003; Noé and Dullo, 2006).

Two living specimens of the calcitic sponge *Acanthochaetetes wellsi* were collected from the Coral Sea near New Caledonia at 8 m water depth (Böhm et al., 1996) and from the Mactan Island near Cebu in the Philippine Islands at

40 m water depth (Reitner et al., 1997). Temperature estimates are from Böhm et al. (1996) and from the World Ocean Atlas (Conkright et al., 1998), respectively.

Two samples were taken from a red coralline algae build-up from Troms/Norway (Freiwald, 1993; Freiwald and Henrich, 1994). One sample has been drilled from a branch of *Lithothamnion glaciale*, the other sample has been drilled from a crust on top of *Lithothamnion glaciale*. The latter sample displays O isotope compositions that are higher by 0.77‰ (Table 1) which may result from changes in salinity and/or temperature or alternatively, this "crust" was segregated by a different algae species. The age of the sample is not constrained but should be Holocene to recent. Accordingly, the water temperature of 7 °C obtained from the World Ocean Atlas (Conkright et al., 1998) should be regarded as an estimate.

From the test of a sea urchin, *Diadema setosum*, an ambulacral plate (#1a) and an interambulacral (#1b) plate were separated. The sample was taken from the fringing reef at the Aqaba Marine Science Station, Gulf of Aqaba, Red Sea. Because *P. lutea* samples were obtained from the same locality, a calcification temperature of about 22 °C is estimated (see Heiss et al., 1999).

Four samples of high-Mg porcelaneous benthic foraminifera were analyzed in this study. *Pyrgo* sp. was collected during a cruise of the research vessel Marion Dufresne from core MD99-2276 at 69°21.94N and 6°32.36W and 2710 m water depth. Its age is uncertain but may correspond to the LGM and the bottom water temperature may have been fairly similar to that today (−1 °C) as estimated from the World Ocean Atlas (Conkright et al., 1998). The single specimen of *Pyrgo rotalaria* was collected from a core top (Meteor cruise core M23341-3, North Atlantic, water depth 1735 m) with a mean annual temperature of −1.0 °C at that site. The single specimen of *Triloculina* sp. and a mixed sample of three porcelaneous specimens are taken from the 250 to 2000 μm size fraction of a Caribbean sediment core sample taken 6 cm below the sediment surface (Meteor cruise core M35019-1, water depth 1815 m). The mean annual temperature at this site is 4.1 °C.

2.1.3. Low-Mg calcite (LMC)

The perforate planktonic foraminifera *Neogloboquadrina dutertrei*, *Globorotalia menardii*, *Globigerinoides sacculifer* and *Globigerinoides ruber* (pink) were picked from the 250 to 315 μm size fraction of a Caribbean core top sample (SO164-04-2) taken during RV Sonne cruise SO164 at 1013 m depth. AMS ^{14}C dating indicates Holocene ages <3000 years for the core top samples (Regenberg et al., 2006). Paleotemperature was calculated according to Anand et al. (2003) from Mg/Ca data obtained from different specimens of the same species and from the same samples.

Neogene coccolith oozes were obtained from ODP Leg 202 Hole 1241A at 2027 m water depth at the Cocos Ridge in the East Pacific (sample P44 at 212.31 m composite depth, 21H-4, 125–127 cm) and ODP Leg 165 Site 1000 at 916 m depth in the Nicaraguan Rise in the Caribbean Sea (sample C56: 105.75 m below sea floor, Hole A 12H-5, 145–147 cm; sample C149: 115.25 meters below sea floor, Hole B, 2R-5, 145–147 cm). The <20 μm sieve fractions were obtained by means of an ethanol rinse. About 66% of all coccoliths in sample P44 were produced by *Reticulofenestra* spp., with a ~14% contribution from the deep dwelling *Florisphaera profunda* and similar amounts of *Sphenolithus* + *Discoaster*. About 43% of coccoliths in sample C149 are derived from *Reticulofenestra* spp., 26% *Umbilicosphaera* spp. and 17% from low-nutrient taxa. The coccolith composition in samples C56 as estimated from a fraction taken 10 cm below appears to be fairly similar to that of C149. Sea surface temperatures are derived from Mg/Ca ratios in foraminifera (Groeneveld, 2005) and ages were modeled according to Steph (2005). For sample C149 a sea surface temperature of 32.8 °C and an age of 3660 ka (Pliocene) is inferred. For sample C56 an age of 3440 ka and a sea surface temperature of 31 °C is derived from bracketing core sections slightly above and below. Sample P44 is of late Miocene age. A rough estimate for the sea surface temperature of about 25 °C is extrapolated from 5.5 Ma old Late Miocene samples about 44 m higher in the same core section (Mix et al., 2003; Groeneveld, 2005).

A test from a brachiopod species, most certainly *Terebratulina* sp., was obtained dead during Meteor RV cruise M61/1-276 at the Belgica Mound province, eastern Porcupine Seabight at 905 m water depth. The ambient water temperature of 9.5 °C was measured in situ with a CTD probe.

2.1.4. Sample cleaning

Apart from JCp-1, all coral, sponge and the red algae sample were obtained by the use of a microdrill, after the outermost surfaces of the specimens had been removed with the drill head to avoid surface contamination.

In order to test the possible effect of organic matrices for Mg isotope analyses, subsamples from the brachiopod test and from the interambulacral plate from *D. setosum* were first powdered in an agate mortar and then bleached for 22 h in 2 ml of 10% NaClO to remove the organic matter. Planktonic and benthic porcelaneous foraminifera were cleaned following published protocols (Barker et al., 2003). Foraminiferal tests were crushed, rinsed with water and methanol, oxidized for 10 min in hot 1% NaOH–0.3% H_2O_2, followed by a short 30 s leach in 0.001 M HNO_3. All cleaning steps were assisted by occasional ultrasonic treatments.

Coccolith oozes P44 and C56 were dissolved in HNO_3 without further treatment, dried down, refluxed with HCl and dried down again. Sample C149 and another aliquot of P44 were cleaned before dissolution. First, 8 ml H_2O (with the pH adjusted to 8.5 by addition of NH_4OH) were added to the samples in centrifuge tubes, the tube shaken and treated with ultrasound for 5 min and then centrifuged. The supernatant was removed using a pipette and the procedure repeated twice. The samples were then oxidized for one hour in a 1:1 mixture of 30% H_2O_2 and 2.8% NaClO. The samples were then centrifuged, the supernatant was removed using a pipette and rinsed eight times with H_2O at pH 8.5 and assisted by ultrasound treatment. Finally, the cleaned coccoliths were transferred to a Savillex beaker in

2.5 ml H_2O and dissolved by the addition of 1 ml 4 M HCl + 0.1 ml H_2O_2.

Generally, up to a few mg of each sample were dissolved in dilute HCl, dried down and redissolved in 250 µl 10 M HCl for chemical purification (Wombacher et al., 2009).

2.2. Analytical methods and notation

The details of the analytical methods are given in Wombacher et al. (2009). Following purification, Mg isotope analyses were conducted using solutions with $\geqslant$50 ng/ml Mg and an Axiom MC-ICP-MS equipped with either a ESI Apex sample inlet system or a glass spray chamber. The standard-sample-bracketing technique was employed for mass bias drift correction. Magnesium stable isotope data is reported as $\delta^{26}Mg = (^{26}Mg/^{24}Mg_{sample}/^{26}Mg/^{24}Mg_{DSM3} - 1) \times 1000$ and as $\delta^{25}Mg = (^{25}Mg/^{24}Mg_{sample}/^{25}Mg/^{24}Mg_{DSM3} - 1) \times 1000$ (Table 1), where DSM3 refers to the currently most widely accepted Mg isotope zero-delta reference (Galy et al., 2003). The $\Delta^{26}Mg$ values in Fig. 1 refer to the Mg isotope fractionation relative to seawater, as calculated by adding 0.8 to the $\delta^{26}Mg$ data reported in Table 1 ($\delta^{26}Mg_{seawater} = -0.8$; Wombacher et al., 2009; Foster et al., 2010 and references therein), except for the speleothem data of Galy et al. (2002), where $\Delta^{26}Mg$ gives the fractionation relative to the corresponding drip waters. Note that modern seawater samples have uniform Mg isotope compositions (Chang et al., 2004; Young and Galy, 2004; de Villiers et al., 2005; Pogge von Strandmann et al., 2008; Tipper et al., 2008; Hippler et al., 2009; Foster et al., 2010) as expected from the long residence times of Mg in the oceans (~13 Ma, Berner and Berner, 1996). The $\delta^{26(25)}Mg'$ (DSM3) notation refers to the alternative δ′-notation of Hulston and Thode (1965) where $\delta^{26(25)}Mg'$ (DSM3) $= 1000 * \ln(\delta^{26(25)}Mg/1000 + 1)$. The δ′-notation facilitates linear mass fractionation lines in three isotope plots. $\Delta^{25}Mg'$ denotes the per mill deviation of the measured $\delta^{25}Mg'$ (DSM3) from the $\delta^{25}Mg'$ calculated from $\delta^{26}Mg'$ (DSM3) using the slope of a linearized three isotope plot that is expected for equilibrium isotope fractionation ($\delta^{25}Mg'$ (calculated) $= 0.521 * \delta^{26}Mg'$ (DSM3); see Young et al., 2002; Young and Galy, 2004).

The external reproducibility of the method is ±0.22 for $\delta^{26}Mg$ (2SD), as estimated from nine repeated separations and a total of 37 Mg isotope analyses from coral reference material JCp-1 throughout this study (Wombacher et al., 2009). The stated reproducibility refers to single 150 s analyses. Procedure blanks ranged from 0.9 to 6.7 ng Mg. Because only 340–680 ng Mg were separated from *L. pertusa* (#1a), *D. dianthus*, *A. willeyana*, *Triloculina* sp., *G. menardii*, *G. sacculifer* and *G. ruber*, the blank may contribute up to 2% of the total Mg. A two percent blank contribution would shift the $^{26}Mg/^{24}Mg$ isotope composition by 0.2‰ if the isotope composition of the blank contribution is different by 10‰ (ca. twice the natural variation), thus a significant blank effect on the Mg isotope composition appears unlikely. A significant erratic blank induced error seems unlikely for two more reasons: (1) the data for *L. pertusa* #1a is within uncertainty similar to a second purification of the same sample (#1b) and the analysis of another *L. pertusa* sample and (2) the data for the foraminifera *G. sacculifer* and *G. ruber* differ only by 0.05‰ and 0.34‰ from the values reported by Pogge von Strandmann (2008), despite the fact that these samples were obtained from different sites and somewhat different cleaning techniques were employed. Note the *G. ruber* of Pogge von Strandmann (2008) was the white morphospecies (pink in this study). Oxygen isotope analyses were carried out for selected samples at the IfM-Geomar/Kiel using a Finnigan MAT252 mass spectrometer with an automated Kiel carbonate preparation device. The results are reported relative to the Vienna PDB scale. The reproducibility derived from eight in-house carbonate standard analyses run along with the samples was ±0.12‰ for $\delta^{18}O$.

3. RESULTS

Magnesium and oxygen isotope data and ambient water temperatures are reported in Table 1. Biogenic aragonite data from cold and warm water coral species and sponges display a fairly constant Mg isotope fractionation relative to seawater without resolvable dependence on ambient water temperature (Fig. 1a). The regression shown in Fig. 1a (dashed line) yields $\Delta^{26}Mg_{aragonite} = 0.001 \pm 0.004 \times T$ (°C) -0.892 ± 0.082 (95% confidence). We choose the format for Fig. 1 and the regression of $\Delta^{26}Mg$ and T (°C) as it allows for intuitive comprehension of this relationship. Given the narrow range in temperatures and the scatter of the data this linear representation is sufficient. However, for (thermodynamic) isotope fractionations, $\alpha - 1$ should scale with $\sim 1/T^2$. Therefore we will also give a scientifically more sound representation of the regressed data: $1000 \times (\alpha_{aragonite} - 1) = -0.005 \pm 0.052 \times 10^6/T^2 - 0.827 \pm 0.613$ (T in K; $\alpha = (\delta^{26}Mg_{CaCO_3}/1000 + 1)/(\delta^{26}Mg_{solution}/1000 + 1)$ with $\delta^{26}Mg_{solution} = -0.80$ if seawater; 95% confidence). Based on the absence of any relationship with temperature, the Mg isotope fractionation is well described by $\Delta^{26}Mg_{coral/sponge\ aragonite} = -0.88 \pm 0.07$ (2 se; $n = 13$) for a temperature range from ~9 to 28 °C. This result is consistent with the analysis of warm water coral aragonite (*Acropora palmata, Acropora* sp. and *Pocillopora* sp.; 22–27.5 °C) by Chang et al. (2004), whose $\Delta^{26}Mg$ values were within -0.8 ± 0.4 and with $\Delta^{26}Mg = -1.0$ for two unspecified corals reported by Dessert et al. (2005). One scaphopod sample by Hippler et al. (2009) (*Antalis costatum*; 20 °C) yields slightly stronger fractionations with $\Delta^{26}Mg = -1.27 \pm 0.05$.

The *Porites* sp. sample JCp-1 with somewhat larger $\Delta^{26}Mg = -1.2$ was excluded from the calculations above, because of the possibility that minor amounts of secondary calcite were present when this reference material was prepared. *Vaceletia* samples were also excluded. Except for *Vaceletia* sp. #2, *Vaceletia* sp. and *V. crypta* display lighter Mg isotope compositions and do not plot onto the aragonite trend. The lightest Vaceletia samples display Mg isotope compositions that are typical for high-Mg calcites. The reason for these variations remains elusive. Tentatively, we suggest secondary high-Mg calcite overgrowths might have altered the initially aragonitic Mg isotope composition, but further investigation is needed.

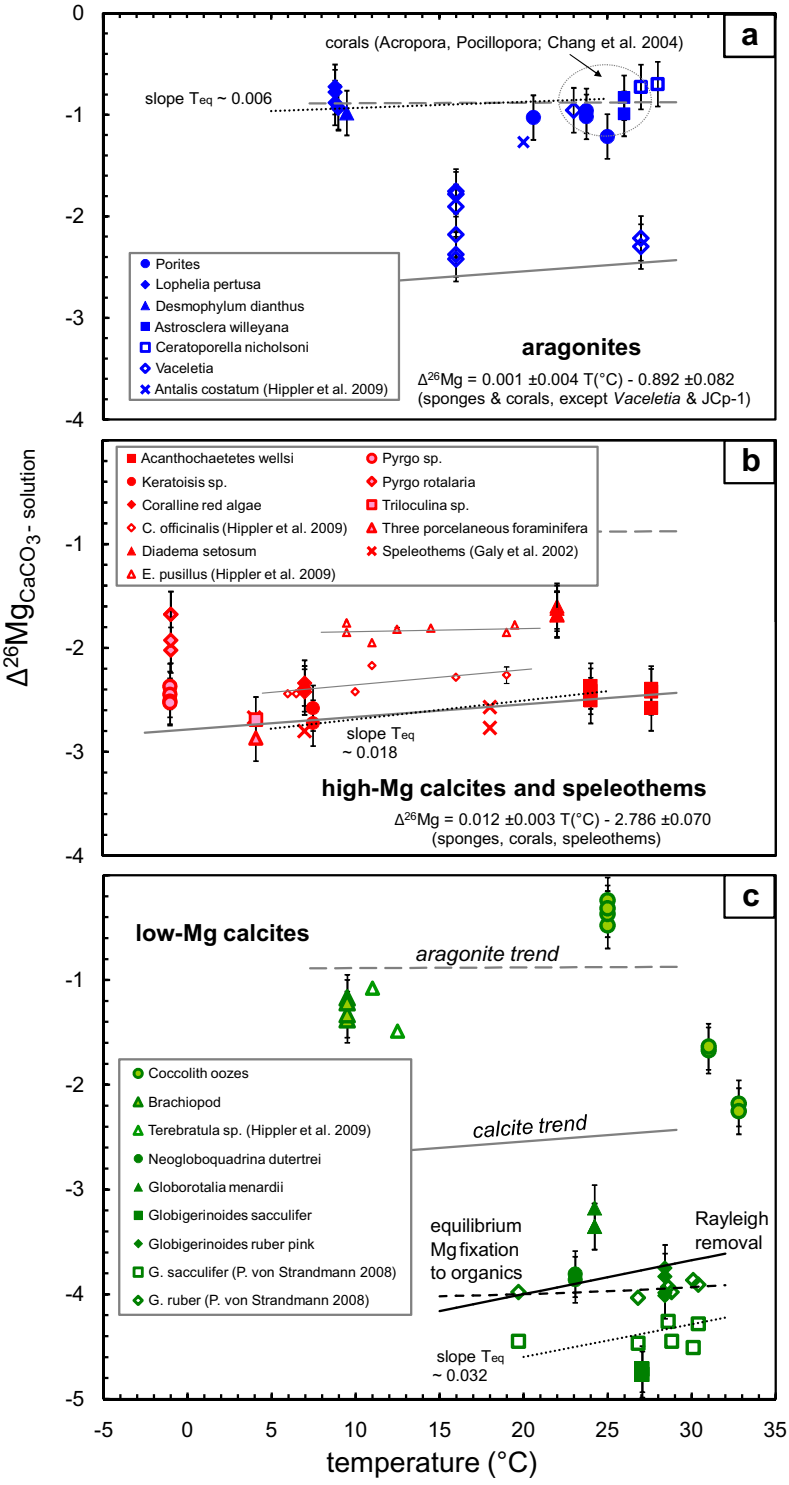

Fig. 1. Magnesium stable isotope compositions for $CaCO_3$ relative to solution vs. temperature. (a) Aragonite samples, (b) high-Mg calcite and speleothems and (c) low-Mg calcite. A seawater Mg isotope composition of $\delta^{26}Mg_{DSM3} = -0.80$ (e.g. Wombacher et al., 2009) was assumed for all data, except for the speleothem data of Galy et al. (2002) which was referenced relative to the corresponding drip water values. Uncertainties refer to the long-term reproducibility (2SD) estimated from 37 analysis of coral reference material JCp-1 (Wombacher et al., 2009), repeated analysis of seawater and a calcitic coral (Pogge von Strandmann, 2008) or 2σ errors from five repetitions measured from the same sample solution (Hippler et al., 2009). The gray dashed line refers to the trend defined by aragonitic corals and sponges from this study, excluding *Vaceletia* and JCp-1. The solid grey line is defined by our calcitic coral and sponge samples and the speleothem data of Galy et al. (2002). The two grey trend lines for *Corallina officinalis* (red algae) and *Echinocyamus pusillus* (echinoid) are defined by the data of Hippler et al. (2009). Stippled lines and slope T_{eq} refer to the temperature dependence for equilibrium isotope fractionation calculated according to Schauble et al. (2009). The solid and dashed black lines in c) refer to Rayleigh removal and equilibrium Mg fixation models for Mg discrimination in foraminifera as discussed in the text. See Section 3 for regressions of the aragonite and high-Mg calcite speleothem Mg isotope data with $1/T^2$.

Like for aragonite corals and sponges, samples from a HMC sclerosponge and an octocoral display a fairly constant fractionation relative to seawater (Fig. 1b) with an average Δ^{26}Mg value of -2.5 ± 0.2. Very similar fractionations are observed for calcitic speleothems Δ^{26}Mg value of -2.7 ± 0.2 (Galy et al., 2002) and another calcitic coral Δ^{26}Mg value of -2.6 ± 0.1 (Pogge von Strandmann, 2008). If we regress the HMC data from the coral and sclerosponge species together with the inorganic speleothem data of Galy et al. (2002), we obtain $\Delta^{26}Mg = 0.012 \pm 0.003 * T$ (°C) -2.786 ± 0.070 or $1000 \times (\alpha_{calcite} - 1) = -0.146 \pm 0.043 \times 10^6/T^2$ (K) -0.836 ± 0.506 (α as defined above; 95% confidence). This regression suggests a weak correlation with temperature. The benthic porcelaneous foraminiferal samples display a ~1‰ range in $^{26}Mg/^{24}Mg$ with coral–sponge–speleothem-like fractionations recorded in a mixed porcelaneous sample ($\Delta^{26}Mg = -2.87$), in *Triloculina* sp. ($\Delta^{26}Mg = -2.69$) and *Pyrgo* sp. ($\Delta^{26}Mg = -2.46 \pm 0.14$; 2SD; $n = 4$) and much weaker fractionations in *P. rotalaria* ($\Delta^{26}Mg = -1.87 \pm 0.36$; 2SD $n = 3$).

From Fig. 1b, it appears that the coralline red algae data (including data of Hippler et al., 2009) is offset to weaker fractionations ($\Delta^{26}Mg = -2.35 \pm 0.19$ (2SD; $n = 9$) compared to the calcitic coral–sclerosponge–speleothem trend. The echinoid data from *D. setosum* and *Echinocyamus pusillus* display much heavier Mg isotope compositions compared to the coral–sponge–speleothem trend with $\Delta^{26}Mg = -1.64 \pm 0.08$ (2SD; $n = 4$) and $\Delta^{26}Mg = -1.83 \pm 0.12$ (2SD; $n = 7$; Hippler et al., 2009). We like to note, that if only HMC data from this study were regressed (with the echinoid and *P. rotalaria* data defined as the only outliers), no relationship between Mg isotope fractionation and temperature would be resolvable ($\Delta^{26}Mg = 0.003 \pm 0.003 \times T$ (°C) -2.54 ± 0.05; 95% confidence). Therefore, the temperature dependence reported here from the regression of coral, sponge and speleothem data should still be viewed with caution. While some porcelaneous foraminifera and echinoids display weaker fractionations with Δ^{26}Mg ranging from −1.6 to −1.9, most biogenic HMC and the speleothems of Galy et al. (2002) fall within -2.6 ± 0.3 for Δ^{26}Mg. In contrast, none of the biogenic LMC samples conform to the ~−2.6‰ fractionation. The brachiopod and coccolith ooze LMC display fractionations weaker than those observed in most HMC samples. The brachiopod $\Delta^{26}Mg = -1.28 \pm 0.19$ (2SD; $n = 4$) compares well with −1.08 and −1.49 observed by Hippler et al. (2009) for *Terebratula* sp. The coccolith oozes span a 2‰ range from $\Delta^{26}Mg = -0.24$ to −2.25 which encompasses the fractionation reported for coccoliths that grew under different laboratory conditions (*E. huxleyi* ($\Delta^{26}Mg = -0.4$‰ to −2.1‰) and *Coccolithus braarudii* ($\Delta^{26}Mg = -0.5$‰ to −1.7‰) (Ra et al., 2010; Müller et al., 2011). The planktonic foraminiferal data ranges from $\Delta^{26}Mg = -3.30$ to −4.74. This compares well with the range of −3.44 to −5.45 in Δ^{26}Mg observed for planktonic and benthic perforate foraminifera by Chang et al. (2004). Moreover, the planktonic foraminifera *N. dutertrei*, *G. sacculifer* and *G. ruber* were also analyzed by Pogge von Strandmann (2008) and our results differ only by +0.08‰, +0.05‰ and −0.34‰, respectively, even though samples were obtained from different sites and somewhat different cleaning techniques were employed. Note *G. ruber* samples of Pogge von Strandmann (2008) refer to the white, our samples to the pink morphospecies.

Bleached sample aliquots from *D. setosum*, coccolith ooze P44 and the brachiopod do not differ from untreated samples outside the analytical uncertainty, which suggests that Mg in residual organic matrices did not significantly contribute to the measured Mg isotope compositions at least in these samples.

4. DISCUSSION

4.1. Magnesium stable isotope fractionation in corals and sclerosponges

4.1.1. Biological influences in coral and sclerosponge calcite and aragonite

As judged from trace elements and stable isotopes, sclerosponges generally appear to precipitate $CaCO_3$ without significant vital effects. While a biological control on trace element incorporation cannot be excluded for the aragonitic *A. willeyana* (Fallon et al., 2005), trace elements and O and C isotopes in the aragonitic *C. nicholsoni* suggest precipitation without obvious biological influences (Druffel and Benavides, 1986; Böhm et al., 2000; Rosenheim et al., 2005). Based on O and C isotopes, Böhm et al. (1996) concluded that *Acanthochaetetes wellsi* precipitates calcite at isotopic equilibrium with ambient seawater. Furthermore, the aragonitic sclerosponges *A. willeyana*, *C. nicholsoni* and *Vaceletia* spp. display Ca isotope compositions that are very similar to those observed for inorganic aragonite precipitation (Gussone et al., 2005).

Compared to sclerosponges, trace element contents and O and C isotope compositions in corals are strongly influenced by biology. Magnesium contents in aragonitic warm and deep water corals including *Porites* and *Desmophyllum* display variations at the microscale that appear to be strongly influenced by the organisms (Hart and Cohen, 1996; Meibom et al., 2004, 2007; Gagnon et al., 2007) and growth rate (e.g. Inoue et al., 2007). Likewise, Thresher et al. (2009) observed irregular Mg/Ca distributions in calcitic bamboo corals including *Keratoisis*. In scleractinian corals, $\delta^{18}O$ is out of equilibrium (McConnaughey, 1989) and displays variations at the small and microscale, as shown for *L. pertusa*, *P. lutea* and *Desmophyllum* (Adkins et al., 2003; Rollion-Bard et al., 2003). The Li isotope composition of corals scatters closely around values observed for inorganically precipitated aragonite (Marriott et al., 2004a; Rollion-Bard et al., 2009; Huang et al., 2010a). Notably, the fractionation in $\Delta^{44/40}$Ca in aragonitic warm water corals including *Acropora* sp. and *Porites* sp. is by about 0.5‰ weaker than in other biogenic or inorganic aragonite samples (Böhm et al., 2006).

4.1.2. Mineralogical control of Mg isotope fractionation in coral and sclerosponge aragonite and calcite

For calcites, the virtually constant Δ^{26}Mg of about −2.6‰ for the high-Mg calcitic coral *Keratoisis* sp., the

sponge samples from *Acanthochaetetes wellsi* and for the speleothems of Galy et al. (2002) (Fig. 1b) suggests that the Mg isotope fractionation recorded in these biogenic high-Mg calcites are representative or very close to the Mg isotope fractionation expected during inorganic calcite precipitation. This is supported by a range of −2.4‰ to −2.8‰ for Δ^{26}Mg relative to the estimated averaged dripwater isotope composition in 16 out of 20 calcitic speleothems reported as group 1 by Immenhauser et al. (2010). However, weaker Mg isotope fractionations were observed in four samples mainly obtained from the surface of speleothems (−1.5‰ to −1.9‰ for Δ^{26}Mg; their group 2), a crystallite from a field precipitation experiment (−1.1‰), and five samples from a laboratory precipitation experiment (−1.6‰ and −2.3‰).

The aragonitic sclerosponges *A. willeyana*, *C. nicholsoni* and one out of three samples of *Vaceletia* sp. display very similar Mg isotope fractionations as the warm and cold water corals *Acropora* sp., *Pocillopora* sp. (Chang et al., 2004), *P. lutea*, *L. pertusa* and *D. dianthus* ($\Delta^{26}Mg = -0.9$; Fig. 1a). The consistent Mg isotope fractionation in coral and sponge aragonite from different species is surprising in the light of the complex and biologically influenced microdistribution of Mg and the presence of biogenic effects on O, C and even Ca isotope compositions in corals. Furthermore, X-ray adsorption fine structure analyses carried out on *Porites*, *Desmophyllum* and *Lophelia* aragonite (Finch and Allison, 2008; Farges et al., 2009) suggest that Mg does not simply substitute for Ca in biogenic coral aragonite, but may be associated with organic matter, an highly disordered inorganic phase or small rhomboedric-carbonate-type environments. Note that Mg in biogenic calcites from rynchonelliform brachiopods and red algae replaces Ca (Cusack et al., 2008; Kamenos et al., 2009). The similar Mg isotope fractionation in coral and sponge aragonites strongly suggest a common Mg isotope fractionation mechanism. Because sponges generally precipitate their skeletons without significant vital effects, $\Delta^{26}Mg = -0.9$ more likely defines inorganic-like Mg isotope fractionation typical for biogenic aragonite precipitation from seawater, even though Mg does not simply substitute for Ca. Note that the Li and Ca isotope fractionations in inorganic aragonite precipitates are similar to biogenic aragonites (Marriott et al., 2004b; Gussone et al., 2005), except for Ca isotopes in corals (Böhm et al., 2006).

Thus it appears that both sponges and corals record inorganic Mg isotope fractionation during aragonite and calcite precipitation, even though coral Mg abundances are typically influenced by biology and Mg in aragonite apparently does not simply substitute for Ca. Nonetheless, additional Mg isotope data on samples from inorganic precipitation experiments and the analysis on inorganic marine cements and more biogenic marine aragonites will be important.

Although there is a clear mineralogical effect on Ca isotope fractionation between most biogenic calcites and aragonites (Gussone et al., 2005), the $^{44}Ca/^{40}Ca$ fractionation in aragonitic warm water corals including *Acropora* sp., and *Porites* sp. is about 0.5‰ weaker than in other biogenic or inorganic aragonites (Böhm et al., 2006). This shift in Ca isotope compositions has been explained in terms of active Ca transport through several cell layers (Böhm et al., 2006). The Mg isotope data may indicate that no significant amount of Mg is actively transported and/or that this transport does not discriminate Mg isotopes. Alternatively, only minor amounts of Mg may be removed from an internal seawater pool during aragonite precipitation, while a significant amount of Ca is removed for $CaCO_3$ formation from such a reservoir. As a consequence, this pool becomes enriched in heavier Ca isotopes and this scenario is consistent with the Rayleigh precipitation model for coral mineralization (Gaetani and Cohen, 2006; Gagnon et al., 2007).

4.2. Cation isotope fractionations in $CaCO_3$

4.2.1. Equilibrium, kinetic chemical and diffusion related isotope fractionations

We will first summarize the mechanisms that can result in particular isotope fractionation patterns during $CaCO_3$ precipitation (see also Fig. 2). Then we will evaluate the data in the context of these mechanisms to derive at a model for cation isotope fractionation during $CaCO_3$ precipitation.

Mass-dependent isotope fractionation under equilibrium conditions results from differences in vibrational frequencies in molecules or condensed phases due to the different masses of the isotopes involved. The heavier isotopes of an element usually become enriched in the phase with the stronger bonds. Equilibrium isotope fractionations are more significant at low temperatures and become negligible at high temperatures (Bigeleisen and Mayer, 1947; Urey, 1947; Schauble, 2004). Kinetic isotope fractionations that result from unidirectional chemical reactions usually enrich the product in the light isotopes. Higher activation energies are needed in order to break bonds involving the heavier isotopes in the reactant phase. Such chemical kinetic fractionations also result from the effect of isotopic mass on vibrational energy, with larger isotope fractiona-

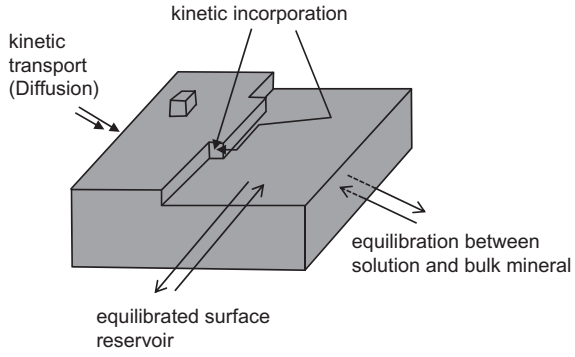

Fig. 2. Sketch showing principle isotope fractionation models for $CaCO_3$ precipitation. Arrows denote forward and back reactions. Two forward arrows for the case of kinetic transport denote isotope fractionations due to differential velocities for (molecules containing) the heavy and light isotopes, respectively. Of all mechanisms depicted, kinetic incorporation best represents crystal growth (e.g. Morse et al., 2007; Raiteri et al., 2010).

tions at low temperature and smaller fractionation at high temperatures (Bigeleisen, 1949). Another class of kinetic isotope fractionations that accompanies diffusion and evaporation results from the differential velocities of isotopically substituted molecules or atoms. Such kinetic transport isotope fractionations are not temperature dependent *per se*, but temperature related changes in the diffusion medium or speciation of the element potentially result in indirect temperature sensitivities. While chemical kinetic isotope fractionations are more likely to be relevant at low temperatures, kinetic transport-related isotope fractionation can be relevant at high and low temperatures (Richter et al., 2009). Note that we refer to kinetic isotope fractionation as the ideal case where reactions proceed unidirectional. Non-equilibrium isotope fractionations refer to reactions that neither proceed under equilibrium nor purely kinetic conditions. The evaporation of water into humid air may be a prime example. In the following, we will evaluate whether equilibrium or kinetic isotope fractionation is consistent with the sign, pattern, temperature and mass-dependence of the observed Mg isotope fractionations.

4.2.2. Sign and pattern of cation isotope fractionation in $CaCO_3$

Light isotope enrichment in $CaCO_3$ relative to the growth solution is a common feature for cation isotope fractionations (Li, Mg, Ca, Fe, Sr, Cd, Ba; e.g. Galy et al., 2002; Wombacher et al., 2003; Marriott et al., 2004b; Gussone et al., 2005; Fietzke and Eisenhauer, 2006; Hathorne and James, 2006; von Blanckenburg et al., 2008; von Allmen et al., 2010). Gussone et al. (2003) argued that the light Ca isotope enrichment in $CaCO_3$ indicates kinetic isotope fractionation due to diffusion of Ca aquocomplexes. In contrast, Marriott et al. (2004b) suggested that the light Li isotope enrichments in $CaCO_3$ were related to the strong 4-fold coordination with water molecules (Yamaji et al., 2001) opposed to the apparently weaker bonds and larger coordination in the mineral structure. Bullen et al. (2003), Lemarchand et al. (2004) and Marriott et al. (2004a) also argued that Ca isotope fractionations in $CaCO_3$ result from equilibrium partitioning. Density-functional electronic structure calculations by Rustad et al. (2010) suggest that equilibrium isotope partitioning between bulk carbonate minerals and solution may enrich light or heavy isotopes depending on the carbonate phase considered, e.g. for calcite they suggest $-5.3‰$ for $\Delta^{26}Mg$ and $+1.5‰$ and $+4.1‰$ for $\Delta^{44/40}Ca$ depending on the coordination of Ca^{2+} in solution. This is in obvious disagreement with data from real samples, e.g. heavy Ca isotope compositions were never reported for calcite. Rustad et al. (2010) suggest that one possible source for the disagreement is that the isotope signature in real samples is imprinted at the interface during the growth processes. Schauble (2011) also estimated equilibrium Mg isotope fractionation between solution and carbonate minerals from first-principles. The results suggest that at room temperature $^{26}Mg/^{24}Mg$ is 3–4‰ lower in carbonate minerals relative to dissolved Mg. This is not unlike but somewhat larger than the observed $\Delta^{26}Mg = -0.9$ and -2.6 for aragonite and calcite. In regard to the inorganic and biological precipitation of carbonate minerals from solution, Schauble (2011) also points out that it is far from clear that equilibrium fractionations are observed and kinetic isotope effects likely contribute to low $\Delta^{26}Mg$ observed in at least some carbonate precipitates. In conclusion, the systematic light isotope enrichment in the mineral phase may be consistent with both, equilibrium and kinetic isotope fractionations but kinetic isotope effects are likely to occur.

Galy et al. (2002) observed a constant offset of about $-2.7‰$ for $\Delta^{26}Mg$ between speleothem calcite and dripwater. They suggested that kinetic (or non-equilibrium effects) will less likely result in reproducible fractionations. Lithium isotopes display constant fractionations in biogenic and inorganic aragonite and calcite independent of the amount of Li incorporation. This was interpreted as an equilibrium rather than kinetic isotope fractionation effect (Marriott et al., 2004a,b). The observation of constant Mg isotope fractionations in calcite (corals, sponges, speleothems, some porcelaneous foraminifera) and aragonite samples is also consistent with equilibrium isotope partitioning. However, bond-breaking chemical kinetic isotope fractionations would also result in constant isotope fractionation factors. For example, the irreversible dehydration of cations during incorporation into $CaCO_3$ could result in a reproducible kinetic isotope fractionation. Note that constant offsets also require the absence of significant reservoir effects, which is consistent with the case of partitioning between a large liquid reservoir and $CaCO_3$. The observed constant offsets for Li, Mg and Ca isotopes in biogenic aragonite and calcite from different species argue against diffusive transport as the cause of the isotope fractionations. This view is further supported by experiments and molecular dynamics simulations that have shown that at least diffusion through water does not result in measurable Mg and only in slightly stronger Ca isotope fractionations (Richter et al., 2006; Bourg and Sposito, 2007; Bourg et al., 2010). Thus, diffusive transport of Mg or Ca to the mineral surface will not result in significant isotope fractionations. While transport-limiting diffusion of components does not result in Mg (and Ca) isotope fractionation, it may affect trace element contents (e.g. Wasylenki et al., 2005).

4.2.3. Temperature-dependence

Schauble et al. (2009) provide the temperature derivative from an approximate formula for equilibrium isotope fractionation given in Bigeleisen and Mayer (1947). Using this expression and typical fractionations of $\Delta^{26}Mg = -2.6$ and -0.9 for calcite and aragonite, respectively, we estimated that $\Delta^{26}Mg$ should decline by 0.006 and 0.018 $°C^{-1}$, respectively, (at 15 °C). This estimated temperature sensitivity is indicated by stippled lines in Fig. 1a and b and is in full accord with the HMC and aragonite data, albeit the scatter in the data is too large to accurately infer the real temperature dependence. For Ca isotopes, the temperature derivative given in Schauble et al. (2009) calculated for inorganically precipitated aragonite ($\Delta^{44}Ca/^{40}Ca \sim -1.7‰$) and foraminiferal calcite ($\Delta^{44}Ca/^{40}Ca \sim -1.1‰$) yields 0.012 and 0.008 $°C^{-1}$, respectively (at 15 °C), which compares to observed values of 0.015 and 0.019 $°C^{-1}$ (Gussone et al., 2003). The aragonite data seems to be in accord

with this estimate, but for calcite there may be some discordance (Schauble et al., 2009; see also calcite data reported in Gussone et al., 2005). The estimates for the equilibrium temperature dependence are in accord with the data (except maybe for Ca isotopes in calcite), but because chemical kinetic stable isotope fractionations may display similar temperature dependences no clear distinction between the two can be made.

4.2.4. Mass-scaling

Because of the larger mass difference of two atomic mass units for $^{26}Mg/^{24}Mg$ compared to only one atomic mass unit for $^{25}Mg/^{24}Mg$, the fractionation exhibited in $^{26}Mg/^{24}Mg$ is about twice that of $^{25}Mg/^{24}Mg$. In detail, however, the mass scaling between the fractionation of the $^{26}Mg/^{24}Mg$ and $^{25}Mg/^{24}Mg$ isotope ratio, i.e. the slope β in a three-isotope plot, differs slightly for equilibrium and kinetic isotope fractionations ($\beta_{eq} = 0.521$; $\beta_{kin} = 0.511$; Young et al., 2002). By definition, equilibrium Mg isotope fractionations are expected to fall along a horizontal line in the $\Delta^{25}Mg'$ vs. $\delta^{26}Mg'$ diagrams introduced by Young and Galy (2004) (Fig. 3).

In Fig. 3 (see Electronic annex EA 1 for $\Delta^{25}Mg'$ and $\delta^{26}Mg'$), the averages of different sample types scatter around the equilibrium fractionation line which they overlap within 2SE in all cases, except for one dolomite sample and two single determinations (rather than averages) for *Keratoisis* sp. Strictly, only *Vaceletia* and CAL-S disagree with the plotted kinetic slopes outside uncertainty and the latter sample is a Upper Jurassic limestone (Yeghicheyan et al., 2003) which is not genetically related to modern ocean water. For carbonate samples, Young and Galy (2004) and Hippler et al. (2009) also observed relationships that are in line with equilibrium isotope fractionation, while Pogge von Strandmann report a slope that differs from the equilibrium slope outside uncertainty; $\beta_{observed} = 0.513 \pm 0.005$). In the evaluation by Young and Galy (2004), carbonate materials and seawater values plot at higher $\Delta^{25}Mg'$ which was interpreted as kinetic isotope fractionation between seawater and the Earth's mantle, a view that is not supported by our data (Fig. 3) and literature data (calculated from data in Foster et al. (2010)). The scatter and disagreement between the data highlights that the determination of slopes in three isotope plots is a matter of precision and accuracy that needs further investigations. However, there are additional factors that need to be taken into account in the interpretation of $\Delta^{25}Mg'$ values as indicators for equilibrium or kinetic isotope fractionation.

Kinetic isotope fractionations are expected to plot to the upper left or lower right of the reactant phase (represented by Mg in modern seawater for most samples here), but kinetic slopes are expected to be variable depending on whether atomic, molecular or reduced masses apply for the calculation of slope β (Young et al., 2002). The dashed reference line in Fig. 3 refers to kinetic fractionations where atomic masses apply. However, in diagrams like Fig. 3, the slope observed for kinetic evaporation of monatomic Cd and Mg into vacuum, a prime example for kinetic fractionation where atomic masses are expected to apply, is about one-third shallower than the predicted kinetic slope for reasons that are not yet understood (see discussion in Wombacher et al. (2008)). Diffusion was already ruled out as the cause of Mg isotope fractionation, but is briefly evaluated for completeness. If dissolved Mg diffuses as part of a molecule, molecular masses apply for the calculation of slope β. The steep kinetic slope in Fig. 3 assumes molecular masses including six water molecules representing the inner hydration sphere of aqueous Mg (Pye and Rudolph, 1998). On the other hand, for diffusion through liquids, reduced masses ($m_{Mg} \times m^*/(m_{Mg} + m^*)$) may apply in which case the slope becomes shallower. Thus $m^*_{(H_2O)} = 18$ could potentially apply for the diffusion of Mg through liquid water

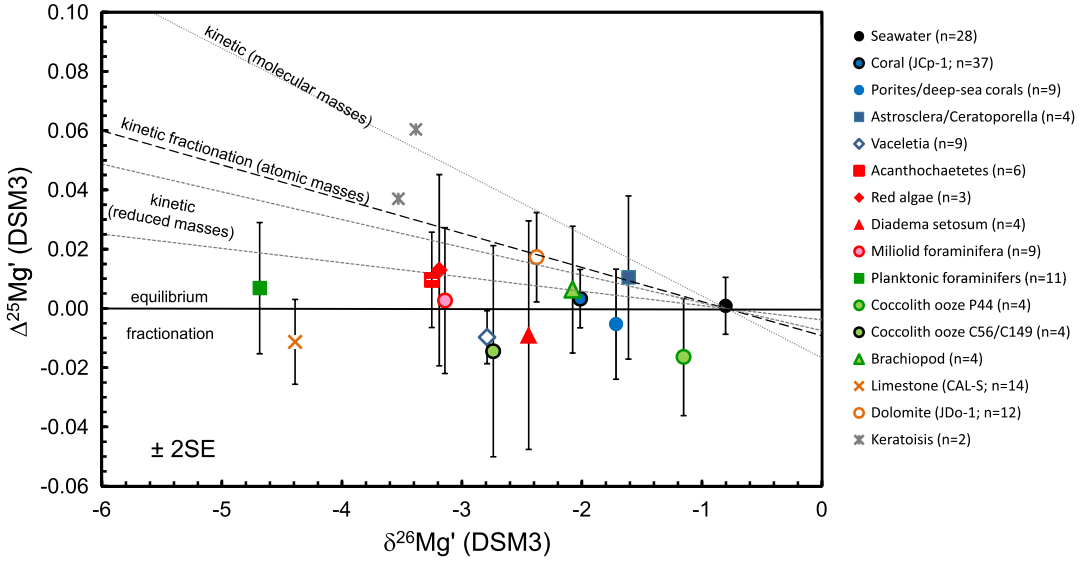

Fig. 3. $\Delta^{25}Mg'$ vs. $\delta^{26}Mg'$ of samples analyzed in this study and additional data for seawater, limestone CAL-S, dolomite JDo-1 and coral JCp-1 from Wombacher et al. (2009). See Section 2.2 for definitions of $\Delta^{25}Mg'$ and $\delta^{26}Mg'$ and Table EA1 (supplement) for data.

which provides the lowest slope in Fig 3. Reduced masses may also apply for bond breaking reactions (Young et al., 2002). Thus, a second dotted line calculated with $m^* = 108$ provides an example for the effect of higher m^* (assuming dehydration of six water molecules). However, any kind of effective reduced masses rather than the exact masses of water molecule or the inner hydration sphere could apply if bonds are broken in unidirectional kinetic reactions. Young et al. (2002) point out that the mass-scaling for kinetic dissociation reactions may be somewhere between that expected for equilibrium and kinetic isotope fractionations. The evaluation of the exact mass-scaling by Young et al. (2002) is derived from mass-dependent stable isotope fractionation theory. However, mass-independent isotope fractionation resulting from nuclear properties potentially complicates this picture. For light elements like Mg nuclear-field shift effects (Bigeleisen, 1996) should be insignificant, but magnetic isotope effects have been detected for Mg (Buchachenko et al., 2005). In summary, the data discussed and shown in Fig. 3 appears to favor equilibrium isotope fractionation, but the accuracy of the results is difficult to prove at the required precision and several complicating factors make such an interpretation immature. Further experimental, theoretical and analytical efforts are needed before such slopes can add substantially to the interpretation of Mg isotope fractionation mechanisms.

4.2.5. Relative equilibrium isotope fractionation between minerals

Marriott et al. (2004b), Gussone et al. (2005), Griffith et al. (2008b) and Huang et al. (2010b) related the heavier Ca (and Li) isotope composition in calcite compared to aragonite or barite to the cation-O bond length and strength within the crystal lattice. This is in agreement with the expectation for equilibrium isotope partitioning, that heavier isotopes should concentrate in phases of low coordination (e.g. Schauble, 2004), i.e. in calcite with 6-fold coordinated cations compared to 9-fold coordination in aragonite. However, this is not the case for Mg isotopes, because light isotopes are more enriched in low-coordinated calcite than aragonite. This observation appears to be in conflict with equilibrium isotope fractionation. However, it may be explained by the suggestion that Mg does not simply substitute for Ca ions in aragonite (Finch and Allison, 2008; Farges et al., 2009). Based on first-principles lattice dynamical modeling of equilibrium isotope effects, Griffith et al. (2008b) suggest that $^{44}Ca/^{40}Ca$ in Ca substituted barite should be about 8‰ lower (at 25 °C) than in calcite, but this difference was not observed in natural and synthetic barite. Thus, these authors suggested that kinetic isotope fractionation processes are involved.

4.3. $CaCO_3$ crystal growth from aqueous solutions

The precipitation of $CaCO_3$ from aqueous solution and thus the transformation of cations from the dissolved state into the crystal lattice requires a series of discrete reaction steps (e.g. De Yoreo and Vekilov, 2003; Morse et al., 2007) that ultimately result in the observed systematic isotope fractionations. In order to infer possible sites where isotope fractionation may occur, we provide a brief qualitative description of the calcite–aqueous solution interface and the steps needed for cation incorporation.

The application of surface X-ray scattering by Geissbühler et al. (2004) and molecular dynamics simulations (e.g. Raiteri et al., 2010) constrain two highly ordered layers of water molecules that form hydrogen bonds with the crystals outermost CO_3^{2-} molecules. Crystal growth from aqueous solutions principally occurs at reactive kink sites at monatomic surface steps that are continuously provided by screw dislocations (Burton et al., 1951). It is commonly expected that cations are transported from the bulk solution to the $CaCO_3$ surface where they adsorb (e.g. Morse et al., 2007; see Fig. 2). Cation adsorption is followed by diffusion parallel to the surface and along steps until the cations become incorporated at reactive kink sites. Using a refined force-field and molecular dynamics simulations, Raiteri et al. (2010) challenged this view and suggest that Ca^{2+} would neither adsorb at calcite surfaces nor diffuse along the crystal interface. Thus Ca^{2+} ions would be incorporated directly from the solution into the kink sites (Fig. 2). Whatever path cations may take, they will finally become incorporated into the crystal at kink sites, where cations and the crystal surface must be desolvated (e.g. Piana et al., 2006) and bonds to CO_3^{2-} ions form. The crystal growth is rate limited either by the integration of cations at reactive sites (Nielsen, 1984; Dove and Czank, 1995; Piana et al., 2006; Kowacz et al., 2007) or by the diffusive flux of constituents (i.e. Ca^{2+} and/or carbonate ions, e.g. Wasylenki et al., 2005).

4.4. Kinetic incorporation model for cation isotope fractionations

Because low temperature $CaCO_3$ precipitation and dissolution are surface controlled processes, it appears unrealistic to assume full isotopic equilibration between the interior crystal lattice and the ambient solution (Fig. 2). Isotope fractionation for Mg and other cations is then either the result of (i) cation adsorption at the crystal surface or (ii) cation incorporation at kink sites. Cations adsorbed at the crystals surface may equilibrate with the cations in the ambient solution. However, adsorbed cations will be only partly dehydrated and at best weakly bond to the crystal surface which appears to be an unlikely cause for the significant fractionations observed. Furthermore, if Raiteri et al. (2010) are correct with their view that Ca ions do not adsorb to the calcite surface, this explanation would be obsolete for Ca isotope fractionation during $CaCO_3$ precipitation and thus another explanation for cation isotope fractionation would be required. In fast growing crystals, incorporation of cations is considered a kinetic process where the desolvation of both cations and the crystal surface is rate-limiting (Nielsen, 1984; Dove and Czank, 1995; Piana et al., 2006; Kowacz et al., 2007). The incorporation at the reactive site including dehydration of cations and the crystal surface and bond formation provides a compelling reason for a chemical kinetic stable isotope fractionation during $CaCO_3$ precipitation. Note that the possible role of dehydration for Li, Mg and Ca isotope

fractionations has been suggested in the literature (Gussone et al., 2003, 2006; Marriott et al., 2004a; Immenhauser et al., 2010; DePaolo, 2011). There is a clear and systematic influence of the mineral structure on Li, Mg and Ca isotope compositions. If the energy barrier of cation dehydration were the only controlling factor, such a mineralogical control would not be expected. However, since the incorporation of cations at kink sites also involves the dehydration of the mineral surface and the formation of new bonds, this mineral specific part of cation incorporation likely affects the activation energy and thus heavy isotope discrimination. Accordingly, we suggest that the mineralogical control on cation isotope fractionations is set by specific mineral surface properties rather than internal crystal properties such as the cation-oxygen bond length and strength (of course, surface properties will to some extent reflect internal crystal properties).

4.5. Calcium and magnesium isotope fractionation models and back reaction

In the following, we discuss previous Ca isotope fractionation models and show how some apparent inconsistencies may be reconciled based on the idea of chemical kinetic isotope fractionations at kink sites. This includes a brief discussion of the effect of back reaction on cation isotope fractionation during $CaCO_3$ precipitation.

Studies of Ca isotope fractionation on biologically and laboratory grown $CaCO_3$ resulted in conflicting interpretations. It has been argued that kinetic Ca isotope fractionation due to diffusion does not explain the temperature dependence observed for Ca isotope fractionation (DePaolo, 2004; Lemarchand et al., 2004). Here, we argue that the mineral-specific offsets for cation stable isotopes observed in many biogenic and inorganic calcite and aragonite samples is difficult to explain by diffusion. Furthermore, experimental and modeling results indicate minor Ca (and no Mg) isotope fractionation due to diffusion in water (Richter et al., 2006; Bourg and Sposito, 2007; Bourg et al., 2010). On the other hand, equilibrium isotope partitioning as the cause for the light Ca isotope enrichment in calcite (Bullen et al., 2003; Lemarchand et al., 2004; Marriott et al., 2004a; Gussone et al., 2005; Sime et al., 2005; Huang et al., 2010b) is inconsistent with the observation by Fantle and DePaolo (2007) that both porewaters and calcite in long-term equilibrium display identical Ca isotope compositions, suggesting an equilibrium isotope fractionation factor of 1.0000 ± 0.0001 for $^{44}Ca/^{40}Ca$). This observation was confirmed by Jacobson and Holmden (2008) and is fully consistent with the suggestion that the light Mg, Ca, Li, etc. isotope enrichment in $CaCO_3$ samples result from kinetic incorporation, i.e. if growth is fast enough for the isotope fractionation to be set by the forward reaction (attachment, precipitation) and back reaction (detachment, dissolution) is insignificant. For the calcite samples of Fantle and DePaolo (2007) and Jacobson and Holmden (2008) where equal precipitation and dissolution fluxes were achieved the net isotope fractionation is reduced to $\Delta^{44}Ca_{eq.} \approx 0‰$ at equilibrium. Fantle and DePaolo (2007) invoked kinetic isotope fractionation which they related to the relative attachment and detachment fluxes of Ca between a postulated interface region and the crystal surface. DePaolo (2011) recently provided a macroscopic model that relates Ca isotope and trace element fractionation in calcite to the balance between the net precipitation rate and the backward reaction rate. Even though the DePaolo model is based on a macroscopic description, he suggests that under conditions dominated by high net precipitation rates, isotope and trace element fractionation is controlled by the kinetics of the ion attachment to the mineral surface and therefore likely related to the kinetics of dehydration. Here, we suggest that kink sites primarily control the detachment and attachment fluxes. As noted above, the fractionation on kink sites allows for the systematic cation isotope fractionations observed in aragonite and calcite samples that are difficult to achieve with kinetic transport processes between an interface region and the crystal surface as in the earlier model of Fantle and DePaolo (2007). Tang et al. (2008) observed stronger light Ca isotope enrichment with increasing precipitation rates and less light isotope enrichment at higher temperature. Tang et al. (2008) invoked the surface entrapment model (SEMO) of Watson (2004) and suggested that the light Ca isotope composition in the surface layer becomes entrapped into the newly formed crystal lattice. Upon slow growth and at higher temperature, diffusive exchange between the uppermost, newly formed crystal surface and the bulk solution resets the Ca isotope composition to about zero fractionation as required by Fantle and DePaolo (2007) model. However, diffusive exchange appears to be inconsistent with the notion that flat (calcite) crystal surfaces are the least favorable site for the dissolution of cations (Spagnoli et al., 2006). Furthermore, if the light surface Ca suggested by Tang et al. (2008) is incorporated at kink sites, it should also contribute to the exchange at the flat surface. These problems are irrelevant, however, if the discrimination against heavy Ca isotopes occurs at the incorporation (kink) site. Partial equilibration at kink (or perhaps step) sites may then result in less isotope fractionation during slow growth and, as suggested by Tang et al. (2008), equilibration may be aided by temperature.

The, at best, weak relationship of Mg isotopes with temperature displayed by the aragonitic and calcitic corals and sclerosponges from this study, the red algae and echinoids of Hippler et al. (2009) and the planktonic foraminifera from Pogge von Strandmann (2008) (Fig. 1) may suggest that back reaction at higher temperatures did not significantly reduce the Mg isotope fractionation and may therefore not be relevant in most biogenic $CaCO_3$ samples. Magnesium isotope fractionation in coccoliths may be affected by back reaction as the fractionation strongly decreases with increasing temperature, but also with the growth rate (Ra et al., 2010).

4.6. Biological effects in high and low-Mg calcite

4.6.1. Potential biological impacts on Mg isotope compositions in calcite

Because the inorganic Mg isotope fractionation during calcite precipitation (about -2.6 for $\Delta^{26}Mg$ at 20 °C) is

now reasonably well constrained, deviations from this trend can be ascribed to biological (or vital) effects. There appear to be five principle causes for biological Mg isotope effects:

(1) Transport to or removal of Mg from the site of $CaCO_3$ precipitation which may involve diffusion through membranes or active pumping (e.g. Erez, 2003; Pogge von Strandmann, 2008; Hippler et al., 2009), in which case light isotopes are expected to be preferentially transported. Rayleigh fractionation is expected if Mg transport occurs in and out of self-contained spaces.
(2) Magnesium may be complexed by biomolecules at the site of precipitation, for example to aid the formation of calcite (e.g. Erez, 2003).
(3) Formation of amorphous calcium carbonate (ACC) as transient precursor phases, such as in sea urchin spicules (e.g. Beniash et al., 1997; Politi et al., 2004). Because Mg may only be partially dehydrated during ACC formation or unfractionated Mg may be trapped within ACC, weaker Mg isotope fractionations are expected.
(4) Changes in the activation barrier for the incorporation of cations in the presence of modifiers. In this regard, Piana et al. (2006) argued that the desolvation of cations and the mineral surface can be assisted by anions adsorbed on the mineral surface. Organic molecules such as peptides can also modify the energy barrier for the integration of solutes in solid phases. For example Stephenson et al. (2008) reported higher Mg contents in calcite if peptides were present and hypothesized that peptides lower the desolvation barrier for Mg relative to that of Ca. It is to be expected that lowering (increasing) the desolvation barrier reduces (increases) the cation isotope fractionation.
(5) Finally, if the ratio of back reaction to forward reaction can be biologically increased, weaker Mg isotope fractionations are to be expected.

4.6.2. High-Mg calcitic foraminifera, echinoids and red algae

Two samples of porcelaneous high-Mg foraminifera, *Triloculina* sp. and a mixed species sample, plot onto the inorganic trend in Fig. 1b. In contrast, *Pyrgo* sp. and especially *P. rotalaria* display heavier isotope compositions. Whether the variable Mg isotope compositions in porcelaneous foraminifera represent real variability or secondary process like partial dissolution (e.g. Towe and Hemleben, 1976) is uncertain and therefore needs to be further investigated. However, the laboratory grown medium-Mg calcite producing benthic foraminifera *Amphistegina* spp. (Eisenhauer et al., 2009) displays weaker than inorganic Mg isotope fractionations similar to *P. rotalaria*, which may suggest that biological effects on Mg isotope compositions in benthic foraminifera are real.

The echinoid data from *D. setosum* and the *E. pusillus* data of Hippler et al. (2009), as well as the red algae data from this study and *Corallina officinalis* (Hippler et al., 2009) display somewhat weaker isotope fractionations than displayed by the "inorganic" coral–sponge–speleothem trend. Inorganically grown calcite accommodates no more than ~8 mol % Mg, because aragonite forms at higher levels of Mg in the growth solution (Glover and Sippel, 1967; Berner, 1975; Gower, 2008). Biogenic calcite, however, can accommodate much higher Mg levels, e.g. in red coralline algae, primary elements of echinoids and some benthic foraminifera. The higher biogenic Mg contents may result from two different strategies that may both involve organic molecules. First, in the presence of hydrophilic peptides, laboratory grown calcite was enhanced in Mg contents by up to 3 mol % (Stephenson et al., 2008). Second, amorphous calcium carbonate (ACC) can be stabilized by proteins in the presence of Mg (Loste et al., 2003; Raz et al., 2003). Beniash et al. (1997) and Politi et al. (2004) observed that sea urchin spicule calcite grows by the transformation of a transient ACC phase. Politi et al. (2004) suggest that the skeletal hard parts of all echinoids form by this process. The weaker than inorganic Mg isotope fractionation in the echinoid high-Mg calcite samples may therefore result from the initial precipitation of amorphous $CaCO_3$. The weaker Mg isotope fractionation could be due to incomplete dehydration or because unfractionated Mg may be trapped within ACC. In fact, one may wonder why there is still such a strong and reproducible Mg isotope fractionation in echinoid calcite. Biogenic ACC appears to contain the order of the prospective crystal polymorph (Hasse et al., 2000; Politi et al., 2006) and may be comparatively dry (Raz et al., 2003; Politi et al., 2004). Such a rather dry and structured material may be able to fractionate Mg isotopes during dehydration and incorporation. To test the suggestion that calcite formation via ACC precursor results in reduced Mg isotope fractionation, laboratory experiments and analyses of biogenic ACC would help.

Evidence of an amorphous precursor phase can be difficult to detect in the presence of the crystalline phase (Gower, 2008). In fact Gower (2008) suggests that high magnesium calcite may be considered a mineralogical signature of probable crystallization via an amorphous precursor. For this reason, we might speculate that the slightly reduced Mg isotope fractionation in the red algae and some benthic foraminifer samples could also be due to a transient amorphous precursor phase. Reduced Mg isotope fractionation due to an amorphous precursor phase suggests that other cations such as Ca also display reduced isotope fractionation effects. With the currently available data, this is difficult to prove or disprove.

4.6.3. Brachiopod and coccolith LMC

Among the low-Mg calcites, the brachiopod and coccolith oozes display "weaker than inorganic" Mg isotope fractionations. The mixed coccolith ooze samples span a range from −2.25 to −0.24 in Δ^{26}Mg. Ra et al. (2010) observed a range from −1.7 to −0.4 for *E. huxleyi* with weaker Mg isotope fractionation at higher temperature and higher growth rate. Here, stronger fractionations are observed for coccoliths that formed under higher temperatures, which tentatively suggests that either different species of coccolithophores display different vital effects or grow at different rates. However, our coccolith oozes could have been contaminated by other shell materials or may be diagenetically

altered, with the Miocene sample P44 ($\Delta^{26}Mg = -0.4 \pm 0.2$) being most susceptible to alteration. Rhynchonelliform brachiopods such as *Terebratulina* analyzed here are characterized by an outer primary layer of fine grained calcite and an inner layer of secondary calcite fibers (Cusack and Freer, 2008). The inner layer is in oxygen isotope equilibrium with seawater and its Mg content reflects the ambient water temperature (Lowenstam, 1961; Perez-Huerta et al., 2008). The cause of the biological effect on Mg isotope fractionation is unclear. It would be interesting to see whether there are differences between the primary and secondary calcite layers.

4.6.4. Planktonic foraminifera

In planktonic foraminifera, biological effects increase the Mg isotope fractionation by 0.8‰ (*G. menardii*) to 2.3‰ (*G. sacculifer*) towards lighter $\delta^{26}Mg$ values compared to the speleothem–sponge–coral trend taken as representative for inorganic calcite precipitation. While Mg substitution in foraminiferal calcite is temperature-dependent (e.g. Nürnberg et al., 1996; Rosenthal et al., 1997), the Mg isotope composition of planktonic foraminifera is not measurably related to temperature (Fig. 1c; Chang et al., 2004; Pogge von Strandmann, 2008). In many biogenic calcites, the increase in Mg abundance with temperature is about three times higher than that expected from thermodynamics and observed in inorganic precipitation experiments (Oomori et al., 1987; Lea et al., 1999; Lea, 2003 and references therein). Relative to inorganic calcite precipitated from seawater, the additional "biological" decrease of Mg contents in foraminiferal calcite is more substantial at low temperatures than at high temperatures. It was suggested that the formation of secondary low-Mg calcite, which contributes the bulk of calcite in planktonic foraminifera, utilizes vacuoles of modified seawater as the source of ions and that the modification of seawater may include the active removal of Mg to allow calcite precipitation (Erez, 2003). Pogge von Strandmann (2008) reasoned that, if Rayleigh-type removal of Mg from vacuoles fractionates Mg isotopes in addition to the ubiquitous inorganic fractionation, the additional biological Mg isotope fractionation (−0.8‰ to −2.3‰) will be less at higher temperatures where comparatively less Mg is removed biologically.

Here, we test this idea using (1) the reported relationship between Mg/Ca and temperature in planktonic foraminifera including *G. ruber* (Mg/Ca [mmol/mol] = $0.52 * e^{0.107T(°C)}$; Elderfield and Ganssen, 2000), (2) the Mg abundances expected for calcite precipitation from unmodified seawater (Mg/Ca [mmol/mol] = $44.5 * e^{0.033T(°C)}$; Oomori et al., 1987), (3) $\Delta^{26}Mg = -4.0$ at 20 °C for *G. ruber* as an example that is representative for most planktonic foraminifera (Pogge von Strandmann, 2008; this study) and (4) the requirement that $^{26}Mg/^{24}Mg$ in the vacuole must be 1.5‰ lighter than seawater due to Mg removal before calcite precipitation commences. Thus, the total fractionation *G. ruber* is −4.0‰, to which the biological Mg removal from vacuoles contributes −1.5‰ and the inorganic fractionation contributes −2.5‰ (at 20 °C). Rayleigh fractionation in the vacuole thus requires that

$$(^{26}Mg/^{24}Mg)_{vacuole}/(^{26}Mg/^{24}Mg)_{seawater} = 0.9985 = f^{\alpha-1} \text{ (at 20 °C)} \quad (1)$$

whereby f is the fraction of Mg remaining in the vacuole and α is the isotope fractionation factor for Mg removal. From the Mg/Ca-temperature relationships given above for foraminiferal and inorganic calcite precipitation, we can calculate $f = 0.045$; i.e. 4.5% at 20 °C. By inserting f into Eq. (1) α can be calculated:

$$\alpha = \ln((^{26}Mg/^{24}Mg)_{vacuole}/(^{26}Mg/^{24}Mg)_{seawater})/\ln(f) + 1 = 1.00048 \quad (2)$$

Using Eq. (1) with $\alpha = 1.00048$ and the remaining Mg fraction f calculated for different temperatures (e.g. 2.3% at 10 °C and 8.7% at 30 °C) yields the curve labeled "Rayleigh removal" plotted in Fig. 1c. The temperature dependence of this curve results from the more substantial Mg removal and thus stronger Mg isotope fractionation at low temperatures. The result is not significantly different if the Mg content of inorganically precipitated calcite were calculated based on data given by Mucci (1987) or if Mg contents were recalculated as concentrations (Mg/(Ca + Mg)) rather than Mg/Ca ratios for the determination of f.

The temperature dependence calculated is not consistent with the available foraminiferal data (Fig. 1c) (even though the slight temperature dependence for the inorganic Mg isotope fractionation was not accounted for). Consequently, simple Rayleigh-type removal of Mg from seawater vacuoles does not account for the low Mg contents of planktonic foraminiferal calcite. We need to stress, however, that the above Rayleigh model requires several assumptions: (1) the seawater–inorganic calcite distribution coefficient and the inorganic calcite fractionation of −2.5‰ for $\Delta^{26}Mg$ (at 20 °C) applies for precipitation from vacuole solutions (Pogge von Strandmann, 2008) and (2) that no additional Ca was pumped into vacuoles and only a small fraction of the vacuole Ca precipitated, as otherwise Mg/Ca in the vacuole would change. However, active pumping of Ca ions into vacuoles was suggested by Erez (2003) and complex internal Ca cycling has been suggested for planktonic and benthic foraminifers (Gussone et al., 2009; Gussone and Filipsson, 2010). While nearly complete precipitation of vacuole Ca were previously suggested by Elderfield et al. (1996), and Kisakürek et al. (2011) suggests that less than half of the Ca supplied by vacuolization precipitated. The possible effects of Ca pumping and precipitation are beyond the scope of this paper, but are potentially relevant for the interpretation of Mg isotope compositions. Erez (2003) pointed out that Mg removal by electrogenic pumps is difficult to envisage, given that Mg is five times more abundant in seawater than Ca and is about 50-fold depleted in planktonic foraminifera. Also Zeebe and Sanyal (2002) argued that Mg removal is energetically less favorable compared to H^+ removal. As an alternative, Erez (2003) suggests the involvement of some organic molecules that complex the Mg and do not let it poison the growth of calcite. If this organic Mg fixation were a unidirectional process and responsible for the stronger Mg isotope frac-

tionation in planktonic foraminifera, it would result in the same curve as shown for Rayleigh removal. If however, the biologically fixed Mg were in equilibrium with the dissolved Mg in the vacuole, we can calculate the isotope composition of the remaining dissolved Mg via mass balance:

$$(^{26}Mg/^{24}Mg)_{vacuole} = (^{26}Mg/^{24}Mg)_{seawater}/(\alpha^{*}_{eq}(1-f)+f) \quad (3)$$

From Eq. (3) with $f = 0.045$ at 20 °C a fractionation factor $\alpha_{eq} = 1.0016$ is derived and with f calculated for different temperatures, $^{26}Mg/^{24}Mg$ for the remaining dissolved Mg in the vacuole is calculated. As evident from Fig. 1c, the "equilibrium organic fixation model" accurately describes the data. However, the assumptions above still apply. Most significantly, the organic Mg fixation model requires the synthesis of large amounts of molecules to dispose huge amounts of Mg which makes it an unlikely scenario.

Stephenson et al. (2008) hypothesized that the rate modifying peptides that increase precipitation rates could also lower the desolvation barrier for Mg incorporation relative to Ca and thereby increase Mg contents. We speculate that, if planktonic foraminifera could utilize biomolecules to actually increase the activation energy for Mg incorporation relative to that of Ca, low Mg contents and increased light Mg isotope enrichment were accounted for and the need to pump out or fix vast amounts of Mg from seawater vacuoles is avoided. Whether such a model can explain species-specific differences in Mg contents and isotope compositions remains to be evaluated further.

5. CONCLUSIONS

A set of Mg isotope data on modern marine biogenic calcite and aragonite samples is reported. Based on these and published data (Galy et al., 2002; Chang et al., 2004; Pogge von Strandmann, 2008; Hippler et al., 2009), we evaluate (i) Mg isotope systematics in biogenic aragonite and calcite, (ii) models for cation isotope fractionation during $CaCO_3$ precipitation, (iii) implications for biomineralization processes in planktonic foraminifera, echinoids, corals and others, and (iv) the potential of Mg isotopes in paleoceanography.

Aragonitic and calcitic sclerosponges and corals precipitate $CaCO_3$ from seawater with mineral-specific Mg isotope fractionations ($\Delta^{26}Mg_{seawater-biogenic\ aragonite} = -0.9 \pm 0.2$; $\Delta^{26}Mg_{seawater-calcite} = -2.6 \pm 0.3‰$). The Mg isotope fractionation in calcite apparently shows a slight dependence on temperature, with weaker fractionations at higher temperature. The observation of mineral-specific offsets in Mg isotope compositions in both, coral and sponge aragonite and calcite suggest an underlying inorganic principle for the Mg isotope fractionation.

5.1. Kinetic incorporation model for cation isotope fractionation

The consideration of isotope fractionation theory and molecular scale crystal growth mechanisms suggests that the observed light cation isotope enrichment in $CaCO_3$ principally is a kinetic isotope effect that results from the incorporation of cations at kink sites. In this model, the mineral-specific kinetic isotope fractionation factors for Li, Mg, Ca, etc. relate to the activation energy required for cation incorporation, which is probably set by cation and surface dehydration and bond formation at the incorporation site. We anticipate that future studies that apply the principles of molecular-scale crystal growth quantitatively and in far more detail will significantly contribute to the understanding of cation isotope fractionation mechanisms.

This kinetic incorporation model predicts several properties for cation isotope fractionation during $CaCO_3$ precipitation, (i) no intrinsic dependence on growth rate, unless significant back reaction upon slow growth reduces the isotope fractionation towards that characteristic for equilibrium isotope partitioning, as may be the case for Ca isotopes in calcite (with $\Delta^{44}Ca_{eq.} \approx 0‰$; Fantle and DePaolo, 2007; Jacobson and Holmden, 2008; Tang et al., 2008; DePaolo, 2011), (ii) a slight decrease of isotope fractionation with increasing temperature (Bigeleisen, 1949), that may be amplified, if higher temperatures promote back reaction and (iii) a sensitivity of cation isotope fractionation to changes in the activation barrier caused by additives such as anions or biomolecules or by the initial precipitation of amorphous $CaCO_3$.

The, at best, weak relationship of Mg isotopes with temperature displayed by the aragonitic and calcitic corals and sclerosponges from this study, the red algae and echinoids of Hippler et al. (2009) and the planktonic foraminifera from Pogge von Strandmann (2008) (Fig. 1) may suggest that back reaction at higher temperatures did not reduce the Mg isotope fractionation appreciably and may therefore not be relevant in most biogenic $CaCO_3$ samples.

5.2. Biological influences on Mg isotope fractionations

Magnesium isotope compositions in low-Mg calcites (planktonic foraminifera, coccoliths, and brachiopods) and some high-Mg calcites (red algae, echinoids, and perhaps some porcelaneous foraminifera) display biological effects that probably relate to the variable strategies employed to precipitate calcite from Mg-rich seawater. While echinoids, red algae, coccolithophores, brachiopods and some benthic foraminifera display weaker than inorganic Mg isotope fractionations, only planktonic foraminifera display stronger light isotope enrichments. The absence of a resolvable temperature sensitivity (Pogge von Strandmann, 2008) for planktonic foraminifera appears to be inconsistent with Mg removal from vacuoles. Fixation of Mg by biomolecules under equilibrium conditions fits the available data. However, we speculate that planktonic foraminifera may be able to synthesize biomolecules that increase the energetic barrier for Mg incorporation. This would be a more cost effective strategy than the fixation or removal of large amounts of Mg.

The observation that coral aragonites display the same Mg isotope fractionation than sclerosponge aragonites is surprising because of the significant biological influence

on trace element and isotope compositions in corals (e.g. McConnaughey, 1989; Hart and Cohen, 1996; Adkins et al., 2003; Rollion-Bard et al., 2003; Meibom et al., 2004, 2007; Böhm et al., 2006; Gagnon et al., 2007). Obviously, the Mg isotope fractionation mechanism is the same for coral and sponge aragonite precipitation. Although Mg in aragonite does not simply substitute for Ca (Finch and Allison, 2008; Farges et al., 2009), it appears most likely that the bulk of the Mg is incorporated into well defined sites rather than associated with organics. Perhaps Mg is incorporated together with an anion that may assist the incorporation in the sense of Piana et al. (2006). For high-Mg calcites like those from red algae and especially for echinoid calcites, the precipitation of amorphous calcium carbonate (ACC) may be a likely cause of weaker Mg isotope fractionations.

5.3. A plea for experiments

Many of the ideas discussed above may be tested and expanded by inorganic precipitation experiments. For aragonite, it would be interesting if (or under which conditions) the fractionation observed in corals and sponges can be reproduced. For cation isotope fractionations (and trace element partitioning) experiments like those of Tang et al. (2008) need to test the effects of growth rates/back reaction and different additives (anions, biomolecules). Perhaps, the contradictory observations of opposite relationships between precipitation rates and Ca isotope fractionations (Lemarchand et al., 2004; Tang et al., 2008) relate to the presence of ammonia in Lemarchand et al. (2004) experiment. Precipitation experiments with amorphous $CaCO_3$ (ACC) would help to test the idea of weaker cation isotope fractionations due to ACC formation. Precipitation in alcohol–water mixtures would allow to better constrain the role of dehydration for cation isotope fractionation. We anticipate that such experiments in combination with further cation isotope studies of biominerals and perhaps soft tissues can add significantly to our comprehension of biomineralization processes and trace element proxies.

5.4. Potential of Mg isotopes for paleoenvironmental reconstructions

As realized from earlier Mg isotope analyses in $CaCO_3$, Mg isotopes offer little if any potential for paleotemperature reconstructions (Galy et al., 2002; Chang et al., 2004; Wombacher et al., 2006; Pogge von Strandmann, 2008; Hippler et al., 2009). Instead it has been suggested that Mg isotopes in $CaCO_3$ can be used to obtain paleo-seawater Mg isotope compositions from which changes in the oceanic Mg cycling throughout the Phanerozoic may be deduced from foraminifera, echinoids or coralline red algae samples (de Villiers et al., 2005; Pogge von Strandmann, 2008; Hippler et al., 2009). We like to caution that high-Mg calcite, aragonite and delicate tests like those of foraminifera are not very stable on geological timescales and therefore may not provide the most robust recorders of past seawater Mg isotope compositions. Possibly, massive low-Mg tests like those of brachiopods may provide better recorders (Veizer et al., 1986; Brand, 2004). This requires that the species to species and intratest variability in such materials, the robustness against diagenesis and the sensitivity of the biological effects to different seawater compositions is constrained.

ACKNOWLEDGMENTS

For sample specimens, support and discussion we thank Joachim Schönfeld, Dirk Nürnberg and Jan Helmke for foraminiferal samples, Sybille Noé for the calcitic coral, Jenny Lezius and Hanno Kinkel for the coccolith oozes and preparation and Gert Wörheide, Helmut Lehnert, Jean Vacelet, Joachim Reitner for sponge samples. André Freiwald for the red algae sample. Thanks to Lulzim Haxhiaj for O isotope analyses and Ana Kolevica for continuous support in the laboratory. We acknowledge the input of the A.E. Edwin Schauble and the reviewers Alex Gagnon, Philip Pogge von Strandmann and Albert Galy and thank Basak Kisakürek for commenting on an earlier draft. The German Science Foundation (DFG) is thanked for funding (MAGISO, Ei272/14-1/2).

APPENDIX A. SUPPLEMENTARY DATA

Supplementary data associated with this article can be found, in the online version, at doi:10.1016/j.gca.2011.07.017.

REFERENCES

Adkins J. F., Boyle E. A., Curry W. B. and Lutringer A. (2003) Stable isotopes in deep-sea corals and a new mechanism for "vital effects". *Geochim. Cosmochim. Acta* **67**, 1129–1143.

Anand P., Elderfield H. and Conte M. H. (2003) Calibration of Mg/Ca thermometry in planktonic foraminifera from a sediment trap series. *Paleoceanography* **18**, 1050. doi:10.1029/2002PA000846.

Astilleros J. M., Fernández-Díaz L. and Putnis A. (2010) The role of magnesium in the growth of calcite: an AFM study. *Chem. Geol.* **271**, 52–58.

Barker S., Greaves M. and Elderfield H. (2003) A study of cleaning procedures used for foraminiferal Mg/Ca paleothermometry. *Geochem. Geophys. Geosyst.* **4**. doi:10.1029/2003GC000559.

Beniash E., Aizenberg J., Addadi L. and Weiner S. (1997) Amorphous calcium carbonate transforms into calcite during sea urchin larval spicule growth. *Proc. R. Soc. Lond. Ser. B* **264**, 461–465.

Berner R. A. (1975) The role of Mg in the crystal growth of calcite and aragonite from sea water. *Geochim. Cosmochim. Acta* **39**, 489–504.

Berner E. K. and Berner R. A. (1996) *Global Environment: Water, Air and Geochemical Cycles*. Prentice-Hall, New Jersey.

Bigeleisen J. (1949) The relative reaction velocities of isotopic molecules. *J. Chem. Phys.* **17**, 675–678.

Bigeleisen J. (1996) Nuclear size and shape effects in chemical reactions. Isotope chemistry of the heavy elements. *J. Am. Chem. Soc.* **118**, 3676–3680.

Bigeleisen J. and Mayer M. G. (1947) Calculation of equilibrium constants for isotopic exchange reactions. *J. Chem. Phys.* **17**, 261–267.

Böhm F., Joachimski M. M., Lehnert H., Morgenroth G., Kretschmer W., Vacelet J. and Dullo W.-C. (1996) Carbon

isotope records from extant Caribbean and South Pacific sponges: evolution of $\delta^{13}C$ in surface water DIC. *Earth Planet. Sci. Lett.* **139**, 291–303.

Böhm F., Joachimski M. M., Dullo W.-C., Eisenhauer A., Lehnert H., Reitner J. and Wörheide G. (2000) Oxygen isotope fractionation in marine aragonite of coralline sponges. *Geochim. Cosmochim. Acta* **64**, 1695–1703.

Böhm F., Haase-Schramm A., Eisenhauer A. and Dullo W.-C. (2002) Evidence for preindustrial variations in the marine surface water carbonate system from coralline sponges. *Geochem. Geophys. Geosyst.* **3**. doi:10.1029/2001GC000264.

Böhm F., Gussone N., Eisenhauer A., Dullo W.-C., Reynaud S. and Paytan A. (2006) Calcium isotope fractionation in modern scleractinian corals. *Geochim. Cosmochim. Acta* **70**, 4452–4462.

Bourg I. C. and Sposito G. (2007) Molecular dynamics simulations of kinetic isotope fractionation during the diffusion of ionic species in liquid water. *Geochim. Cosmochim. Acta* **71**, 5583–5589.

Bourg I. C., Richter F. M., Christensen J. N. and Sposito G. (2010) Isotopic mass dependence of metal cation diffusion coefficients in liquid water. *Geochim. Cosmochim. Acta* **74**, 2249–2250.

Brand U. (2004) Carbon, oxygen and strontium isotopes in Paleozoic carbonate components: an evaluation of original seawater-chemistry proxies. *Chem. Geol.* **204**, 23–44.

Buchachenko A. L., Kouznetsov D. A., Orlova M. A. and Markarian A. A. (2005) Magnetic isotope effect of magnesium in phosphoglycerate kinase phosphorylation. *Proc. Natl. Acad. Sci. USA* **102**, 10793–10796.

Buhl D., Immenhauser A., Smeulders G., Kabiri L. and Richter D. K. (2007) Time series $\delta^{26}Mg$ analysis in speleothem calcite: kinetic versus equilibrium fractionation, comparison with other proxies and implications for palaeoclimate research. *Chem. Geol.* **244**, 715–729.

Bullen T. D., Kim S. T. and Paytan A. (2003) Ca isotope fractionation during Ca-carbonate precipitation: there's more to it than temperature. *Geochim. Cosmochim. Acta* **67**, A49.

Burton W. K., Cabrera N. and Frank F. C. (1951) The growth of crystals and the equilibrium structure of their surfaces. *Philos. Trans. R. Soc. Lond. Ser. A* **243**, 299–358.

Chang V. T.-C., Makishima A., Belshaw N. S. and O'Nions R. K. (2003) Purification of Mg from low-Mg biogenic carbonates for isotope ratio determination using multiple collector ICP-MS. *J. Anal. At. Spectrom.* **18**, 296–301.

Chang V. T.-C., Williams R. J. P., Makishima A., Belshaw N. and ÓNions R. K. (2004) Mg and Ca isotope fractionation during $CaCO_3$ biomineralisation. *Biochem. Biophys. Res. Commun.* **323**, 79–85.

Conkright M., Levitus S., O'Brian T., Boyer T., Antonov J. and Stephens C. (1998) World ocean atlas 1998 CD-ROM data set documentation. Technical Report 15. NODC Internal Report, Silver Spring, MD.

Cusack M. and Freer A. (2008) Biomineralization: elemental and organic influence in carbonate systems. *Chem. Rev.* **108**, 4433–4454.

Cusack M., Pérez-Huerta A., Janousch M. and Finch A. A. (2008) Magnesium in the lattice of calcite-shelled brachiopods. *Chem. Geol.* **257**, 59–64.

Davis K. J., Dove P. M. and De Yoreo J. (2000) The role of Mg^{2+} as an impurity in calcite growth. *Science* **290**, 1134–1137.

de Villiers S., Dickson J. A. D. and Ellam R. M. (2005) The composition of the continental river weathering flux deduced from seawater Mg isotopes. *Chem. Geol.* **216**, 133–142.

De Yoreo J. J. and Vekilov P. G. (2003) Principles of crystal nucleation and growth. In *Biomineralization* (eds. P.M. Dove, J.J. DeYoreo and S. Weiner), Rev. Min. Geochem. Vol. 54, Min. Soc. Am., Washington, pp. 57–93.

DePaolo D. J. (2004) Calcium isotopic variations produced by biological, kinetic, radiogenic and nucleosynthetic processes. In *Geochemistry of Non-traditional Stable Isotopes*, vol. 55 (eds. C. M. Johnson, B. L. Beard and F. Albarède), pp. 255–288. Rev. Min. Geochem.. Min. Soc. Am., Washington.

DePaolo D. J. (2011) Surface kinetic model for isotopic and trace element fractionation during precipitation of calcite from aqueous solutions. *Geochim. Cosmochim. Acta* **75**, 1039–1056.

Dessert C., Galy A. and Elderfield H. (2005) Mechanisms of Mg isotopes fractionation during $CaCO_3$ biomineralisation. *Geochim. Cosmochim. Acta* **69**, A214.

Dove P. M. and Czank C. A. (1995) Crystal chemical controls on the dissolution kinetics of the isostructural sulfates: celestite, anglesite, and barite. *Geochim. Cosmochim. Acta* **59**, 1907–1915.

Druffel E. R. M. and Benavides L. M. (1986) Input of excess CO_2 to the surface ocean based on $^{13}C/^{12}C$ ratios in a banded Jamaican sclerosponge. *Nature* **321**, 58–61.

Eisenhauer A., Kisakürek B. and Böhm F. (2009) Marine calcification: an alkali earth metal isotope perspective. *Elements* **5**, 365–368.

Elderfield H. and Ganssen G. (2000) Past temperature and $\delta^{18}O$ of surface ocean waters inferred from foraminiferal Mg/Ca ratios. *Nature* **405**, 442–445.

Elderfield H., Bertram C. J. and Erez J. (1996) A biomineralization model for the incorporation of trace elements into foraminiferal calcium carbonate. *Earth Planet. Sci. Lett.* **142**, 409–423.

Erez J. (2003) The source of ions for biomineralization in foraminifera and their implications for paleooceanographic proxis. In *Biomineralization* (eds. P.M. Dove, J.J. DeYoreo and S. Weiner) Rev. Min. Geochem. Vol. 54, Min. Soc. Am., Washington, pp. 115–149.

Fallon S. J., McCulloch M. T. and Guilderson T. P. (2005) Interpreting environmental signals from the coralline sponge *Astrosclera willeyana*. *Palaeogeogr. Palaeoclimatol. Palaeoecol.* **228**, 58–69.

Fantle M. S. and DePaolo D. J. (2007) Ca isotopes in carbonate sediment and pore fluid from ODP Site 807A: the $Ca^{2+}(aq)$-calcite equilibrium fractionation factor and calcite recrystallization rates in Pleistocene sediments. *Geochim. Cosmochim. Acta* **71**, 2524–2546.

Farges F., Meibom A., Flank A.-M., Lagarde P., Janousch M. and Stolarski J. (2009) Speciation of Mg in biogenic calcium carbonates. *J. Phys. Conf. Ser.* **190**, 012175.

Fietzke J. and Eisenhauer A. (2006) Determination of temperature-dependent stable strontium isotope ($^{88}Sr/^{86}Sr$) fractionation via bracketing standard MC-ICP-MS. *Geochem. Geophys. Geosyst.* **7**, Q08009. doi:10.1029/2006GC001243.

Finch A. A. and Allison N. (2008) Mg structural state in coral aragonite and implications for the paleoenvironmental proxy. *Geophys. Res. Lett.* **35**, L08704.

Flügel E. (2004) *Microfacies of Carbonate Rocks: Analysis, Interpretation and Application*. Springer, Berlin.

Foster G. L., Pogge von Strandmann P. A. E. and Rae J. W. B. (2010) Boron and magnesium isotopic composition of seawater. *Geochem. Geophys. Geosyst.* **11**, Q08015.

Freiwald A. (1993) Coralline algal maerl frameworks – islands within the phaeophytic kelp belt. *Facies* **29**, 133–148.

Freiwald A. and Henrich R. (1994) Reefal coralline algal build-ups within the Arctic Circle: morphology and sedimentary dynamics under extreme environmental seasonality. *Sedimentology* **41**, 963–984.

Gaetani G. A. and Cohen A. L. (2006) Element partitioning during precipitation of aragonite from seawater: a framework for

understanding paleoproxies. *Geochim. Cosmochim. Acta* **70**, 4617–4634.

Gagnon A. C., Adkins J. F., Fernandez D. P. and Robinson L. F. (2007) Sr/Ca and Mg/Ca vital effects correlated with skeletal architecture in a scleractinian deep-sea coral and the role of Rayleigh fractionation. *Earth Planet. Sci. Lett.* **261**, 280–295.

Galy A., Belshaw N. S., Halicz L. and ÓNions R. K. (2001) High-precision measurement of magnesium isotopes by multiple-collector inductively coupled plasma mass spectrometry. *Int. J. Mass Spectrom.* **208**, 89–98.

Galy A., Bar-Matthews M., Halicz L. and ÓNions R. K. (2002) Mg isotopic composition of carbonate: insight from spelothem formation. *Earth Planet. Sci. Lett.* **201**, 105–115.

Galy A., Yoffe O., Janney P. E., Williams R. W., Cloquet C., Alard O., Halicz L., Wadhwa M., Hutcheon I. D., Ramon E. and Carignan J. (2003) Magnesium isotope heterogeneity of the isotopic standard SRM980 and new reference materials for magnesium-isotope-ratio measurements. *J. Anal. At. Spectrom.* **18**, 1352–1356.

Geissbühler P., Fenter P., DiMasi E., Srajer G., Sorensen L. B. and Sturchio N. C. (2004) Three-dimensional structure of the calcite–water interface by surface X-ray scattering. *Surf. Sci.* **573**, 191–203.

Glover E. D. and Sippel R. F. (1967) Synthesis of magnesium calcites. *Geochim. Cosmochim. Acta* **31**, 603–613.

Gower L. B. (2008) Biomimetic model systems for investigating the amorphous precursor pathway and its role in biomineralization. *Chem. Rev.* **108**, 4551–4627.

Griffith E. M., Paytan A., Kozdon R., Eisenhauer A. and Ravelo A. C. (2008a) Influences on the fractionation of calcium isotopes in planktonic foraminifera. *Earth Planet. Sci. Lett.* **268**, 124–136.

Griffith E. M., Schauble E. A., Bullen T. D. and Paytan A. (2008b) Characterization of calcium isotopes in natural and synthetic barite. *Geochim. Cosmochim. Acta* **72**, 5641–5658.

Groeneveld J. (2005) Effect of the Pliocene closure of the Panamanian Gateway on Caribbean and east Pacific sea surface temperatures and salinities by applying combined Mg/Ca and $\delta^{18}O$ measurements (5.6–2.2 Ma). Ph.D Thesis, Universität Kiel.

Gussone N. and Filipsson H. L. (2010) Calcium isotope ratios in calcitic tests of benthic foraminifers. *Earth Planet. Sci. Lett.* **290**, 108–117.

Gussone N., Eisenhauer A., Heuser A., Dietzel M., Bock B., Böhm F., Spero H. J., Lea D., Bijma J. and Nägler T. F. (2003) Model for kinetic effects on Ca isotope fractionation ($\delta^{44}Ca$) in inorganic aragonite and cultured planktonic foraminifera. *Geochim. Cosmochim. Acta* **67**, 1375–1382.

Gussone N., Böhm F., Eisenhauer A., Dietzel M., Heuser A., Teichert B. M. A., Reitner J., Wörheide G. and Dullo W.-C. (2005) Calcium isotope fractionation in calcite and aragonite. *Geochim. Cosmochim. Acta* **69**, 4485–4494.

Gussone N., Langer G., Thoms S., Nehrke G., Eisenhauer A., Riebesell U. and Wefer G. (2006) Cellular calcium pathways and isotope fractionation in *Emiliania huxleyi*. *Geology* **34**, 625–628.

Gussone N., Hönisch B., Heuser A., Eisenhauer A., Spindler M. and Hemleben C. (2009) A critical evaluation of calcium isotope ratios in tests of planktonic foraminifers. *Geochim. Cosmochim. Acta* **73**, 7241–7255.

Hardie L. A. (1996) Secular variations in seawater chemistry: an explanation for the coupled secular variation in the mineralogies of marine limestones and potash evaporites over the past 600 m.y. *Geology* **24**, 279–283.

Hart S. R. and Cohen A. L. (1996) An ion probe study of annual cycles of Sr/Ca and other trace elements in corals. *Geochim. Cosmochim. Acta* **60**, 3075–3084.

Hasse B., Ehrenberg H., Marxen J. C., Becker W. and Epple M. (2000) Calcium carbonate modifications in the mineralized shell of the freshwater snail Biomphalaria glabrata. *Chem. Eur. J.* **6**, 3679–3685.

Hathorne E. C. and James R. H. (2006) Temporal record of lithium in seawater: a tracer for silicate weathering? *Earth Planet. Sci. Lett.* **246**, 393–406.

Heiss G. A., Dullo W.-C., Joachimski M. M., Reijmer J. J. G. and Schuhmacher H. (1999) Increased seasonality in the Gulf of Aqaba, Red Sea, recorded in the oxygen isotope record of a *Porites lutea* coral. *Senkenbergiana Marit.* **30**, 17–26.

Higgins J. A. and Schrag D. P. (2010) Constraining magnesium cycling in marine sediments using magnesium isotopes. *Geochim. Cosmochim. Acta* **74**, 5039–5053.

Hippler D., Buhl D., Witbaard R., Richter D. K. and Immenhauser A. (2009) Towards a better understanding of magnesium-isotope ratios from marine skeletal carbonates. *Geochim. Cosmochim. Acta* **73**, 6134–6146.

Hoernle K., Mortimer N., Werner R. and Hauff F. (eds.) (2003) RV SONNE cruise report SO168. ZEALANDIA. Geomar report 113, Kiel/Germany, 127pp.

Huang K.-F., You C.-F., Liu Y.-H., Wang R.-M., Lin P.-Y. and Chung C.-H. (2010a) Low-memory, small sample size, accurate and high-precision determinations of lithium isotopic ratios in natural materials by MC-ICP-MS. *J. Anal. At. Spectrom.* **25**, 1019–1024.

Huang S., Farkas J. and Jacobsen S. B. (2010b) Calcium isotopic fractionation between clinopyroxene and orthopyroxene from mantle peridotites. *Earth Planet. Sci. Lett.* **292**, 337–344.

Hulston J. R. and Thode H. G. (1965) Variations in the S^{33}, S^{34}, and S^{36} contents of meteorites and their relation to chemical and nuclear effects. *J. Geophys. Res.* **70**, 3475–3484.

Immenhauser A., Buhl D., Richter D., Niedermayr A., Riechelmann D., Dietzel M. and Schulte U. (2010) Magnesium-isotope fractionation during low-Mg calcite precipitation in a limestone cave – field study and experiments. *Geochim. Cosmochim. Acta* **74**, 4346–4364.

Inoue M., Suzuki A., Nohara M., Hibino K. and Kawahata H. (2007) Empirical assessment of coral Sr/Ca and Mg/Ca ratios as climate proxies using colonies grown at different temperatures. *Geophys. Res. Lett.* **34**, L12611. doi:10.1029/2007GL029628.

Jacobson A. D. and Holmden C. (2008) $\delta^{44}Ca$ evolution in a carbonate aquifer and its bearing on the equilibrium isotope fractionation factor for calcite. *Earth Planet. Sci. Lett.* **270**, 349–353.

Kamenos N. A., Cusack M., Huthwelker T., Lagarde P. and Scheibling R. E. (2009) Mg-lattice associations in red coralline algae. *Geochim. Cosmochim. Acta* **73**, 1901–1907.

Kasemann S. A., Schmidt D. N., Pearson P. N. and Hawkesworth C. J. (2008) Biological and ecological insights into Ca isotopes in planktic foraminifers as a palaeotemperature proxy. *Earth Planet. Sci. Lett.* **271**, 292–302.

Kisakürek B., Eisenhauer A., Böhm F., Hathorne E. C. and Erez J. (2011) Controles on calcium isotope fractionation in cultured planktic foraminifera, *Globigerinoides ruber* and *Globigerinella siphonifera*. *Geochim. Cosmochim. Acta* **75**, 427–443.

Kowacz M., Putnis C. V. and Putnis A. (2007) The effect of cation:anion ratio in solution on the mechanism of barite growth at constant supersaturation: role of the desolvation process on the growth kinetics. *Geochim. Cosmochim. Acta* **71**, 5168–5179.

Langer G., Gussone N., Nehrke G., Riebesell U., Eisenhauer A. and Thoms S. (2007) Calcium isotope fractionation during coccolith formation in *Emiliania huxleyi*: independence of growth and calcification rate. *Geochem. Geophys. Geosyst.* **8**, Q05007. doi:10.1029/2006GC001422.

Lea D. W. (2003) Elemental and isotopic proxis of past ocean temperatures. In *Treatise on Geochemistry* (eds. H. D. Holland and K. K. Turekian). Elsevier, pp. 365–390.

Lea D. W., Mashiotta T. A. and Spero H. J. (1999) Controls on magnesium and strontium uptake in planktonic foraminifera determined by live culturing. *Geochim. Cosmochim. Acta* **63**, 2369–2379.

Lemarchand D., Wasserburg G. J. and Papanastassiou D. A. (2004) Rate-controlled calcium isotope fractionation in synthetic calcite. *Geochim. Cosmochim. Acta* **68**, 4665–4678.

Loste E., Wilson R. M., Seshadri R. and Meldrum F. C. (2003) The role of magnesium in stabilising amorphous calcium carbonate and controlling calcite morphologies. *J. Cryst. Growth* **254**, 206–218.

Lowenstam H. A. (1961) Mineralogy, $^{18}O/^{16}O$ ratios, and strontium and magnesium contents of recent and fossil brachiopods and their bearing on the history of the oceans. *J. Geol.* **69**, 241–260.

Marriott C. S., Henderson G. M., Belshaw N. S. and Tudhope A. W. (2004a) Temperature dependence of δ^7Li, δ^{44}Ca and Li/Ca during growth of calcium carbonate. *Earth Planet. Sci. Lett.* **222**, 615–624.

Marriott C. S., Henderson G. M., Crompton R., Staubwasser M. and Shaw S. (2004b) Effect of mineralogy, salinity, and temperature on Li/Ca and Li isotope composition of calcium carbonate. *Chem. Geol.* **212**, 5–15.

McConnaughey T. (1989) ^{13}C and ^{18}O isotopic disequilibrium in biological carbonates: I. Patterns. *Geochim. Cosmochim. Acta* **53**, 151–162.

Meibom A., Cuif J.-P., Hillion F., Constantz B. R., Juillet-Leclerc A., Dauphin Y., Watanabe T. and Dunbar R. B. (2004) Distribution of magnesium in coral skeleton. *Geophys. Res. Lett.* **31**, L23306.

Meibom A., Mostefaoui S., Cuif J.-P., Dauphin Y., Houlbreque F., Dunbar R. and Constantz B. (2007) Biological forcing controls the chemistry of reef-building coral skeleton. *Geophys. Res. Lett.* **34**, L02601.

Mix A. C., Tiedemann R., Blum, P., et al. (2003) *Proceedings of the Ocean Drilling Program, Initial Reports* **202**.

Morse J. W., Arvidson R. S. and Lüttge A. (2007) Calcium carbonate formation and dissolution. *Chem. Rev.* **107**, 342–381.

Mucci A. (1987) Influence of temperature on the composition of magnesian calcite overgrowths precipitated from seawater. *Geochim. Cosmochim. Acta* **51**, 1977–1984.

Mucci A. and Morse J. W. (1984) The solubility of calcite in seawater solutions of various magnesian concentration, $I_t = 0.697$ m at 25 °C and one atmosphere total pressure. *Geochim. Cosmochim. Acta* **48**, 815–822.

Müller M. N., Kisakürek B., Buhl D., Gutperlet R., Kolevica A., Riebesell U., Stoll H. and Eisenhauer A. (2011) Response of the coccolithophores *Emiliania huxleyi* and *Coccolithus braarudii* to changing seawater Mg^{2+} and Ca^{2+} concentrations: Mg/Ca, Sr/Ca ratios and $\delta^{44/40}$ Ca, $\delta^{26/24}$ Mg of coccolith calcite. *Geochim. Cosmochim. Acta* **75**, 2088–2102.

Nägler T. F., Eisenhauer A., Müller A., Hemleben C. and Kramers J. (2000) The δ^{44} Ca-temperature calibration on fossil and cultured *Globigerinoides sacculifer*: new tool for reconstruction of past sea surface temperatures. *Geochem. Geophys. Geosyst.* **23**, 2000GC000091.

Nielsen A. E. (1984) Electrolyte crystal growth mechanisms. *J. Cryst. Growth* **67**, 289–310.

Noé S. and Dullo W.-C. (2006) Skeletal morphogenesis and growth mode of modern and fossil deep-water isidid gorgonians (Octocorallia) in the West Pacific (New Zealand and Sea of Okhotsk). *Coral Reefs* **25**, 303–320.

Nürnberg D., Bijma J. and Hemleben C. (1996) Assessing the reliability of magnesium in foraminiferal calcite as a proxy for water mass temperatures. *Geochim. Cosmochim. Acta* **60**, 803–814.

Okai T., Suzuki A., Kawahata H., Terashima S. and Imai N. (2003) Preparation of a new geological survey of Japan geochemical reference material: coral JC_P-1. *Geost. Newslett.* **26**, 95–99.

Oomori T., Kaneshima H., Maezato Y. and Kitano Y. (1987) Distribution coefficient of Mg^{2+} ions between calcite and solution at 10–50 °C. *Mar. Chem.* **20**, 327–336.

Perez-Huerta A., Cusack M., Jeffries T. E. and Williams C. T. (2008) High resolution distribution of magnesium and strontium and the evaluation of Mg/Ca thermometry in recent brachiopod shells. *Chem. Geol.* **247**, 229–241.

Piana S., Jones F. and Gale J. D. (2006) Assisted desolvation as a key kinetic step for crystal growth. *J. Am. Chem. Soc.* **128**, 13568–13574.

Pogge von Strandmann P. A. E. (2008) Precise magnesium isotope measurements in core top planktic and benthic foraminifera. *Geochem. Geophys. Geosyst.* **9**, Q12015. doi:10.1029/2008GC002209.

Pogge von Strandmann P. A. E., James R. H., van Calsteren P., Gíslason S. R. and Burton K. W. (2008) Lithium, magnesium and uranium isotope behaviour in the estuarine environment of basaltic islands. *Earth Planet. Sci. Lett.* **274**, 462–471.

Politi Y., Arad T., Klein E., Weiner S. and Addadi L. (2004) Sea urchin spine calcite forms via a transient amorphous calcium carbonate phase. *Science* **306**, 1161–1164.

Politi Y., Levi-Kalisman Y., Raz S., Wilt F., Addadi L., Weiner S. and Sagi I. (2006) Structural characterization of the transient amorphous calcium carbonate precursor phase in sea urchin embryos. *Adv. Funct. Mater.* **16**, 1289–1298.

Pye C. C. and Rudolph W. W. (1998) An ab initio and Raman investigation of magnesium(II) hydration. *J. Phys. Chem. A* **102**, 9933–9943.

Ra K., Kitagawa H. and Shiraiwa Y. (2010) Mg isotopes in chlorophyll-a and coccoliths of cultured coccolithophores (*Emiliania huxleyi*) by MC-ICP-MS. *Mar. Chem.* **122**, 130–137.

Raiteri P., Gale J. D., Quigley D. and Rodger P. M. (2010) Derivation of an accurate force-field for simulating the growth of calcium carbonate from aqueous solution: a new model for the calcite–water interface. *J. Phys. Chem. C* **114**, 5997–6010.

Raz S., Hamilton P. C., Wilt F. H., Weiner S. and Addadi L. (2003) The transient phase of amorphous calcium carbonate in sea urchin larval spicules: the involvement of proteins and magnesium ions in its formation and stabilization. *Adv. Funct. Mater.* **13**, 480–486.

Regenberg M., Nürnberg D., Steph S., Groeneveld J., Garbe-Schönberg D., Tiedemann R. and Dullo W.-C. (2006) Assessing the effect of dissolution on planktonic foraminiferal Mg/Ca ratios: evidence from Caribbean core tops. *Geochem. Geophys, Geosyst.* **7**, Q07P15. doi:10.1029/2005GC001019.

Reitner J., Wörheide G., Lange R. and Thiel V. (1997) Biomineralization of calcified skeletons in three Pacific coralline demosponges – an approach to the evolution of basal skeletons. *Cour. Forsch. Inst. Senckenberg* **201**, 371–383.

Richter F. M., Mendybaev R. A., Christensen J. N., Hutcheon I. D., Williams R. W., Sturchio N. C. and Beloso J. A. D. (2006) Kinetic isotopic fractionation during diffusion of ionic species in water. *Geochim. Cosmochim. Acta* **70**, 277–289.

Richter F. M., Dauphas N. and Teng F.-Z. (2009) Non-traditional fractionation of non-traditional isotopes: evaporation, chemical diffusion and Soret diffusion. *Chem. Geol.* **258**, 92–103.

Rollion-Bard C., Blamart D., Cuif J. P. and Juillet-Leclerc A. (2003) Microanalysis of C and O isotopes of azooxanthellate and zooxanthellate corals by ion microprobe. *Coral Reefs* **22**, 405–415.

Rollion-Bard C., Vigier N. and Spezzaferri S. (2007) In situ measurements of calcium isotopes by ion microprobe in carbonates and application to foraminifera. *Chem. Geol.* **244**, 679–690.

Rollion-Bard C., Vigier N., Meibom A., Blamart D., Reynaud S., Rodolfo-Metalpa R., Martin S. and Gattuso J.-P. (2009) Effect of environmental conditions and skeletal ultrastructure on the Li isotopic composition of scleractinian corals. *Earth Planet. Sci. Lett.* **286**, 63–70.

Rose-Koga E. F. and Albarède F. (2010) A data brief on magnesium isotope compositions of marine calcareous sediments and ferromanganese nodules. *Geochem. Geophys. Geosyst.* **11**, Q03006. doi:10.1029/2009GC002899.

Rosenheim B. E., Swart P. K. and Thorrold S. R. (2005) Minor and trace elements in sclerosponge *Ceratoporella nicholsoni*: biogenic aragonite near the inorganic endmember. *Palaeogeogr. Palaeoclimatol. Palaeoecol.* **228**, 109–129.

Rosenthal Y., Boyle E. A. and Slowey N. C. (1997) Temperature control on the incorporation of magnesium, strontium, fluorine, and cadmium into benthic foraminiferal shells from Little Bahama Bank; prospects for thermocline paleoceanography. *Geochim. Cosmochim. Acta* **61**, 3633–3643.

Rüggeberg A., Fietzke J., Liebetrau V., Eisenhauer A., Dullo W.-C. and Freiwald A. (2008) Stable strontium isotopes ($\delta^{88/86}Sr$) in cold-water corals – a new proxy for reconstruction of intermediate ocean water temperatures. *Earth Planet. Sci. Lett.* **269**, 569–574.

Rustad J. R., Casey W. H., Yin Q.-Z., Bylaska E. J., Felmy A. R., Bogatko S. A., Jackson V. E. and Dixon D. A. (2010) Isotopic fractionation of Mg^{2+}(aq), Ca^{2+}(aq), and Fe^{2+}(aq) with carbonate minerals. *Geochim. Cosmochim. Acta* **74**, 6301–6323.

Schauble E. A. (2004) Applying stable isotope fractionation theory to new systems. In *Geochemistry of non-traditional stable isotopes* (eds. C. M. Johnson, B. L. Beard and F. Albarède) Rev. Min. Geochem. Vol. 55, Min. Soc. Am., Washington, pp. 65–111.

Schauble E. A. (2011) First-principles estimates of equilibrium magnesium isotope fractionation in silicate, oxide, carbonate and hexaaquamagnesium(2+) crystals. *Geochim. Cosmochim. Acta* **75**, 844–869.

Schauble E. A., Méheut M. and Hill P. S. (2009) Combining metal stable isotope fractionation theory with experiments. *Elements* **5**, 369–374.

Sime N. G., De La Rocha C. L. and Galy A. (2005) Negligible temperature dependence of calcium isotope fractionation in 12 species of planctonic foraminifera. *Earth Planet. Sci. Lett.* **232**, 51–66.

Skulan J., DePaolo D. J. and Owens T. L. (1997) Biological control of calcium isotopic abundances in the global calcium cycle. *Geochim. Cosmochim. Acta* **61**, 2505–2510.

Spagnoli D., Kerisit S. and Parker S. C. (2006) Atomistic simulation of the free energies of dissolution of ions from flat and stepped calcite surfaces. *J. Cryst. Growth* **294**, 103–110.

Stanley S. M. (2006) Influence of seawater chemistry on biomineralization throughout phanerozoic time: paleontological and experimental evidence. *Palaeogeo. Palaeoclimatol. Palaeolecol.* **232**, 214–236.

Steph S. (2005) Pliocene stratigraphy and the impact of Panama uplift on changes in Caribbean and tropical east Pacific upper ocean stratification (6–2.5 Ma). Ph.D. Thesis, Universität Kiel.

Stephenson A. E., DeYoreo J. J., Wu L., Wu K. J., Hoyer J. and Dove P. M. (2008) Peptides enhance magnesium signature in calcite: insights into origins of vital effects. *Science* **322**, 724–727.

Tang J., Dietzel M., Böhm F., Köhler S. J. and Eisenhauer A. (2008) Sr^{2+}/Ca^{2+} and $^{44}Ca/^{40}Ca$ fractionation during inorganic calcite formation: II. Ca isotopes. *Geochim. Cosmochim. Acta* **72**, 3733–3745.

Thresher R. E., MacRae C. M., Wilson N. C. and Fallon S. (2009) Feasibility of age determination of deep-water bamboo corals (Gorgonacea; Isididae) from annual cycles in skeletal composition. *Deep Sea Res. Part I* **56**, 442–449.

Tipper E. T., Louvat P., Capmas F., Galy A. and Gaillardet J. (2008) Accuracy of stable Mg and Ca isotope data obtained by MC-ICP-MS using the standard addition method. *Chem. Geol.* **257**, 65–75.

Towe K. M. and Hemleben C. (1976) Diagenesis of magnesian calcite: evidence from miliolacean foraminifera. *Geology* **4**, 337–339.

Tucker M. (2001) *Sedimentary Petrology: An Introduction to the Origin of Sedimentary Rocks*. Blackwell Science, Oxford.

Urey H. C. (1947) The thermodynamic properties of isotopic substances. *J. Chem. Soc.*, 562–581.

Veizer J., Fritz P. and Jones B. (1986) Geochemistry of brachiopods: oxygen and carbon isotopic records of Paleozoic oceans. *Geochim. Cosmochim. Acta* **50**, 1679–1696.

von Allmen K., Böttcher M. E., Samankassou E. and Nägler T. F. (2010) Barium isotope fractionation in the global barium cycle: first evidence from barium minerals and precipitation experiments. *Chem. Geol.* **277**, 70–77.

von Blanckenburg F., Mamberti M., Schoenberg R., Kamber B. S. and Webb G. E. (2008) The iron isotope composition of microbial carbonate. *Chem. Geol.* **249**, 113–128.

Wasylenki L. E., Dove P. M. and De Yoreo J. J. (2005) Effects of temperature and transport conditions on calcite growth in the presence of Mg^{2+}: implications for paleothermometry. *Geochim. Cosmochim. Acta* **69**, 4227–4236.

Watson E. B. (2004) A conceptual model for near-surface kinetic controls on the trace-element and stable isotope composition of abiotic calcite crystals. *Geochim. Cosmochim. Acta* **68**, 1473–1488.

Wombacher F., Rehkämper M., Mezger K. and Münker C. (2003) Stable isotope compositions of cadmium in geological materials and meteorites determined by multiple-collector ICPMS. *Geochim. Cosmochim. Acta* **67**, 4639–4654.

Wombacher F., Eisenhauer A., Böhm F., Gussone N., Kinkel H., Lezius J., Noé S., Regenberg M. and Rüggeberg A. (2006) Magnesium stable isotope compositions in biogenic $CaCO_3$. European Geoscience Union, *Geophys. Res. Abstr.* **8**, p. 06353.

Wombacher F., Rehkämper M., Mezger K., Bischoff A. and Münker C. (2008) Cadmium stable isotope cosmochemistry. *Geochim. Cosmochim. Acta* **72**, 646–667.

Wombacher F., Eisenhauer A., Heuser A. and Weyer S. (2009) Separation of Mg, Ca and Fe from geological reference materials for stable isotope ratio analyses by MC-ICP-MS and double-spike TIMS. *J. Anal. At. Spectrom.* **24**, 627–636.

Wörheide G. (1998) The reef cave dwelling ultraconservative coralline demosponge *Astrosclera willeyana* Lister 1900 from the Indo-Pacific. *Facies* **38**, 1–88.

Yamaji K., Makita Y., Watanabe H., Sonoda A., Kanoh H., Hirotsu T. and Ooi K. (2001) Theoretical estimation of lithium

isotopic reduced partition function ratio for lithium ions in aqueous solution. *J. Phys. Chem. A* **105**, 602–613.

Yeghicheyan D., Carignan J., Valladon M., Bouhnik Le Coz M., Samuel J., BenBakkar M., Bruguier O., Keller F., Pin C., Pourtales L., Hénin O., Macè J., Morin N., Guilmette C. and Marin L. (2003) The new carbonate reference material CAL-S: preliminary results. *Abs. Geoanal.*, **146** (abstr.).

Young E. D. and Galy A. (2004) The isotope geochemistry and cosmochemistry of magnesium. In *Geochemistry of non-traditional stable isotopes* (eds. C. M. Johnson, B. L. Beard and F. Albarède) Rev. Min. Geochem. Vol. 55, Min. Soc. Am., Washington, pp. 197–230.

Young E. D., Galy A. and Nagahara H. (2002) Kinetic and equilibrium mass-dependent isotope fractionation laws in nature and their geochemical and cosmochemical significance. *Geochim. Cosmochim. Acta* **66**, 1095–1104.

Zeebe R. E. and Sanyal A. (2002) Comparison of two potential strategies of planktonic foraminifera for house building: Mg^{2+} or H^{+} removal? *Geochim. Cosmochim. Acta* **66**, 1159–1169.

Associate editor: Edwin A. Schauble